

AD-A122 209

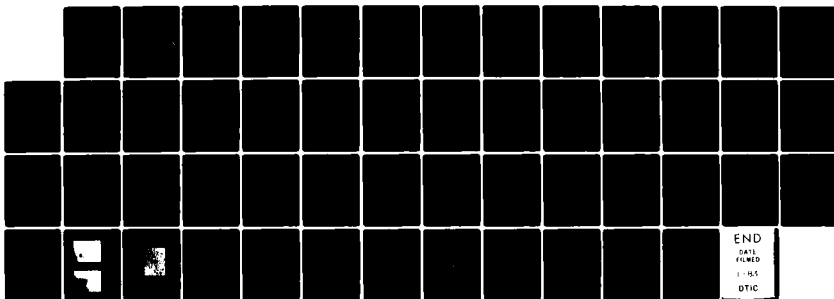
RESEARCH ON MOLECULAR BEAM EPITAXY(U) VARIAN ASSOCIATES
INC PALO ALTO CA Y-CHAI ET AL. MAY 82 AFOSR-TR-82-1033
F49620-81-C-0068

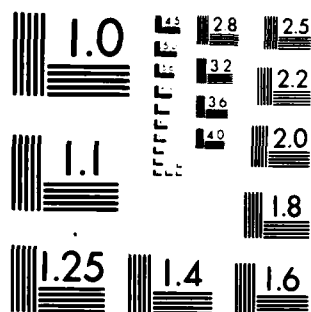
1/1

UNCLASSIFIED

F/G 20/2

NL





MICROCOPY RESOLUTION TEST CHART
NATIONAL BUREAU OF STANDARDS 1963-A

AFOSR-TR. 82-1033



AD A122209

RESEARCH ON MOLECULAR BEAM EPITAXY

FINAL SCIENTIFIC REPORT
(Period 1 May 1981 -- 30 April 1982)

May 1982

Sponsored by:

Air Force Office of Scientific Research
Bolling AFB, Washington, DC 20332



Contract F49620-81-C-0068

Approved for public release;
distribution unlimited.

Y. Chai and R. Chow

Varian Associates, Inc.
Solid State Laboratory
Palo Alto, CA 94303

DTIC FILE COPY

92 12 09 034

UNCLASSIFIED

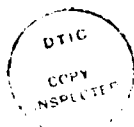
SECURITY CLASSIFICATION OF THIS PAGE (When Data Entered)

REPORT DOCUMENTATION PAGE		READ INSTRUCTIONS BEFORE COMPLETING FORM
1. REPORT NUMBER AFOSR-TR- 82 - 1033	2. GOVT ACCESSION NO. AD-A122209	3. RECIPIENT'S CATALOG NUMBER
4. TITLE (and Subtitle) Research on Molecular Beam Epitaxy		5. TYPE OF REPORT & PERIOD COVERED Final Report May 1981 -- April 1982
		6. PERFORMING ORG. REPORT NUMBER
7. AUTHOR(s) Y. G. Chai and R. Chow		8. CONTRACT OR GRANT NUMBER(s) F49620-81-C-0068
9. PERFORMING ORGANIZATION NAME AND ADDRESS Varian Associates, Inc. 611 Hansen Way Palo Alto, CA 94303		10. PROGRAM ELEMENT, PROJECT, TASK AREA & WORK UNIT NUMBERS 00-00000 61102F 000000 2305/C1
11. CONTROLLING OFFICE NAME AND ADDRESS Director, Air Force Office of Scientific Research Attn: NE, Bldg. 410 Bolling AFB, Washington, DC 20332		12. REPORT DATE May 1982
14. MONITORING AGENCY NAME & ADDRESS (if different from Controlling Office)		13. NUMBER OF PAGES 51
		15. SECURITY CLASS. (of this report) Unclassified
15a. DECLASSIFICATION DOWNGRADING SCHEDULE		
16. DISTRIBUTION STATEMENT (of this Report) Approved for public release; distribution unlimited		
17. DISTRIBUTION STATEMENT (of the abstract entered in Block 20, if different from Report)		
18. SUPPLEMENTARY NOTES		
19. KEY WORDS (Continue on reverse side if necessary and identify by block number) phosphine MBE-InP Cracking Tantalum Thermal dissociation		
20. ABSTRACT (Continue on reverse side if necessary and identify by block number) Thermodynamic calculations show that phosphine should thermally dissociate into the phosphorus dimer to a high degree. Three furnaces were constructed to study the cracking of phosphine. Phosphine was found to react with tantalum, but not to any great extent with quartz. Cracking efficiencies greater than 90% were obtained with the furnace using a quartz cartridge filled with matted quartz. Molecular beam epitaxial layers of InP were grown on Cr-doped, (100)-oriented InP substrates using the quartz cartridge		

UNCLASSIFIED

SECURITY CLASSIFICATION OF THIS PAGE(When Data Entered)

furnace. The 77°K photoluminescence spectra were comparable to other MBE InP using other types of phosphorus sources. Carrier mobility and concentrations at 77°K and 300°K were measured.



Accession For	
NTIS GRA&I	
DTIC TAB	
Unannounced	
Justification	
By _____	
Distribution/	
Availability Codes	
Dist	Avail and/or Special
A	

SECURITY CLASSIFICATION OF THIS PAGE(When Data Entered)



TABLE OF CONTENTS

<u>Section</u>		<u>Page</u>
I.	INTRODUCTION	1
II.	THEORETICAL	2
III.	EXPERIMENTAL	8
	A. System Design for Cracking Experiments	8
	B. Safety Aspects of Using Phosphine	8
	C. Cracking Furnaces	12
	D. Experimental Conditions	14
	E. System for Growth Experiments	18
IV.	RESULTS AND DISCUSSION	20
	A. Cracker Furnace	20
	B. Materials Characterization	33
V.	SUMMARY	40
VI.	REFERENCES	41
	APPENDIX A: HANDLING OF COMPRESSED PH_3 GAS CYLINDERS	42

AIR FORCE OFFICE OF SCIENTIFIC RESEARCH (AFSC)
NOTICE OF REVIEW OF THIS REPORT
This report has been reviewed and is
approved for release under E.O. 12958-2.
Distribution is unlimited.
MATTHEW J. H. [illegible]
Chief, Technical Information Division



I. INTRODUCTION

The semiconductor InP is important for the development of millimeter-wave Gunn devices for use in "smart missile" guidance up to 100 GHz and higher. InP epilayers are also needed as confining or window layers in InGaAs and InGaAsP light emitters and detectors. Also, InP has the potential for high-velocity FET material for millimeter-wave FETs.

InP molecular beam epitaxy (MBE) started as early as 1974 [1-3]. In most cases, either InP chips or elemental phosphorus (P_4) were used as a phosphorus source. The disadvantage of using InP chips is that they become progressively indium-rich as phosphorus evaporates, and the source requires frequent recharging. When elemental phosphorus is used, the evaporated phosphorus condenses as a white phosphorus which is highly inflammable and toxic. The exposure of this condensed white phosphorus to oxygen can cause fire or even explosions. Also, accurate control of the phosphorus vapor pressure may be difficult because the phosphorus furnace temperature must be low due to its high vapor pressure, and radiative heating and cooling are very sluggish at low temperatures.

Under the present program, we proposed the use of gaseous phosphine (PH_3) as a phosphorus source. Gas in a cylinder provides an effectively inexhaustible supply of phosphorus, and the gas flow can be controlled rapidly and accurately using an ultra-high vacuum leak valve. Gaseous PH_3 can be converted into hydrogen (H_2) and phosphorus (P_2 or P_4) molecules by pyrolysis. Therefore, bleeding PH_3 from a gas tank into the MBE system through a high-temperature cracking furnace should provide the phosphorus molecular beam required for InP MBE.



II. THEORETICAL

Thermal decomposition of PH_3 occurs according to the equations:



The equilibrium constants of the above reactions obtained from Ref. 4 are plotted in Fig. 1 as a function of temperature. We can see that the formation of the monomer, P , is at least a thousand times less likely than the formation of P_2 and P_4 . Also, the reaction constant, k_1 , is high at low temperatures, but k_2 is high at temperatures above 1200°C . In both cases, the equilibrium constants k_1 and k_2 always show a high degree of PH_3 decomposition into the phosphorus molecules (P_2 and P_4) at temperatures above 600°C .

Given a mixture of P_2 and P_4 in the furnace hot zone, we determined which of these species is thermodynamically favored. The equilibrium constant of the reaction



is

$$k_4 = [\text{P}_2]^2/[\text{P}_4] \quad .$$

Therefore,

$$\log [\text{P}_2]/[\text{P}_4] = \log k_4 - \log [\text{P}_2] \quad . \quad (5)$$

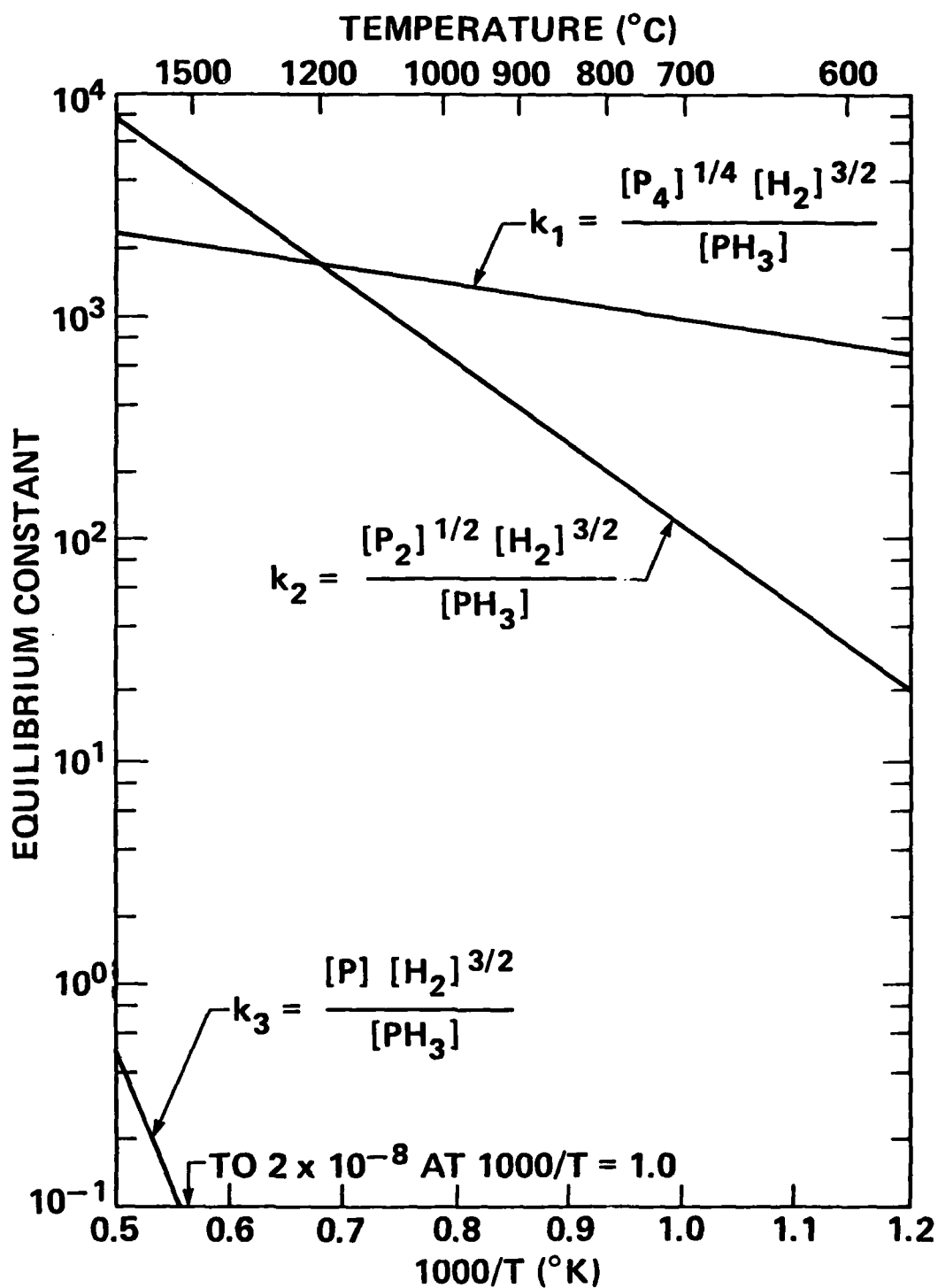


Fig. 1 Equilibrium constants k_1 , k_2 and k_3 versus inverse temperature for the dissociation of PH_3 into P_4 , P_2 and P , respectively.



The ratio $[P_2]/[P_4]$ is plotted for three different P_2 partial pressures, 10^{-8} , 10^{-6} , and 10^{-4} atmospheres in Fig. 2, using the thermodynamic data from Ref. 4.

For GaAs MBE, a typical vapor pressure of As_4 is 10^{-8} atm (7.6×10^{-6} Torr) for 1-micron/hour growth rate. Similarly, we expected to obtain a phosphorus-stabilized InP surface when the P_2 pressure was in the range of 10^{-8} atm. As can be seen from Fig. 2, the ratio $[P_2]/[P_4]$ was already larger than unity at a temperature of only 400°C and reached 10^7 at about 1000°C at $P_2 = 10^{-8}$ atm. This means that cracking of P_4 into P_2 is virtually complete at about 1000°C . Even at higher P_2 pressures of 10^{-4} atm, the $[P_2]/[P_4]$ ratio is still as high as 1000 near 1000°C . So if we assume equilibrium conditions when P_2 and P_4 pass through the furnace hot zone at a temperature of 1000°C , the gas mixture should convert completely to P_2 .

Now we consider the equilibrium constant of reaction (2) as a function of pressure. The equilibrium constant is

$$k_2 = [P_2]^{1/2}[H_2]^{3/2}/[PH_3] \quad (6)$$

Since the decomposition of PH_3 produces three times more H_2 molecules than P_2 , the partial pressure of H_2 can be approximated by

$$[H_2] = 3[P_2] \quad (7)$$

at the high temperatures and low pressures existing in the cracking furnace. Substituting Eq. (7) into Eq. (6) and rearranging to obtain the ratio $[P_2]/[PH_3]$ gives

$$\log [P_2]/[PH_3] = \log k_2 - 1.5 \log 3 - \log [P_2] \quad (8)$$

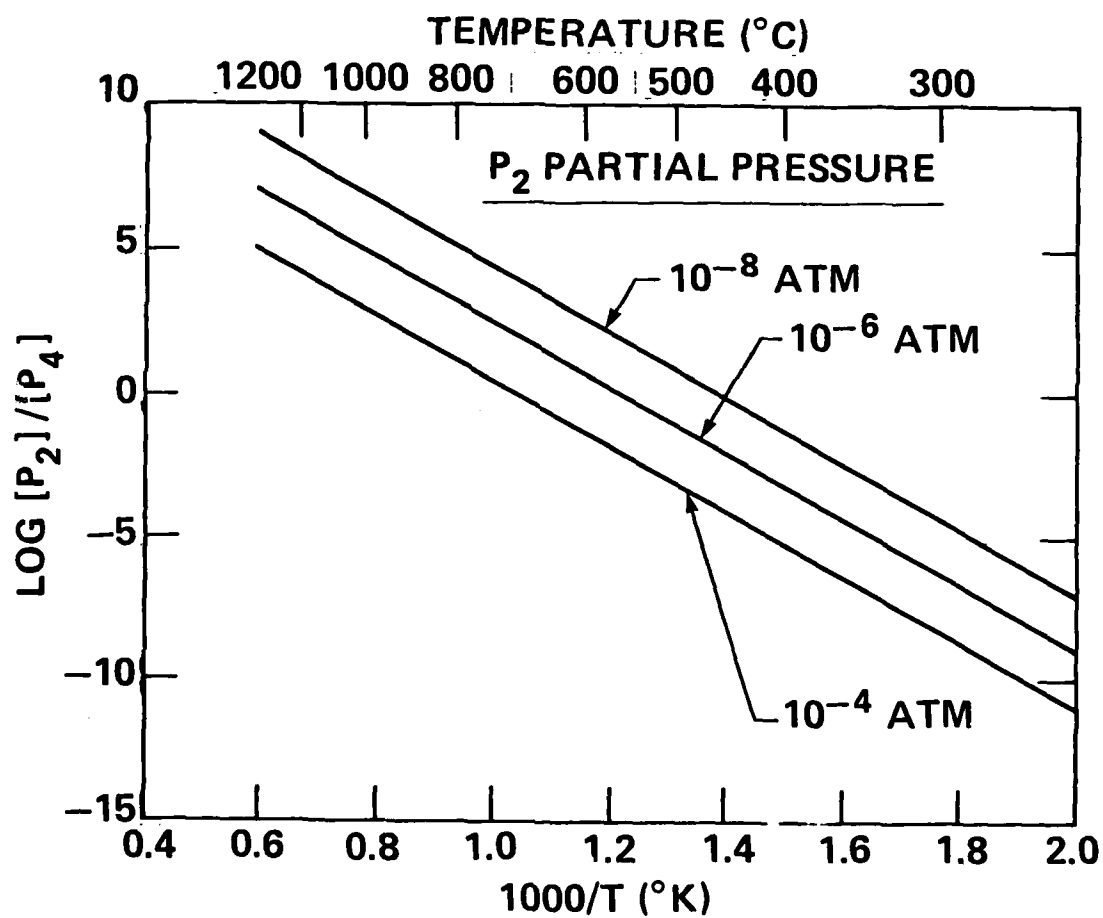


Fig. 2 $[P_2]/[P_4]$ partial pressure ratio versus inverse temperature at three P_2 partial pressures. $[P_2]/[P_4]$ is greater than one at temperatures higher than 800°C for a given pressure.



Figure 3 shows a plot of Eq. (8) for partial pressures of $P_2 = 10^{-8}$, 10^{-6} and 10^{-4} atm. It is seen that the ratio $[P_2]/[PH_3]$ is greater than 10^4 for all cases, indicating that the decomposition of PH_3 is complete.

This analysis is for equilibrium conditions only, and indicates qualitative trends that may occur by cracking PH_3 in a vacuum furnace.

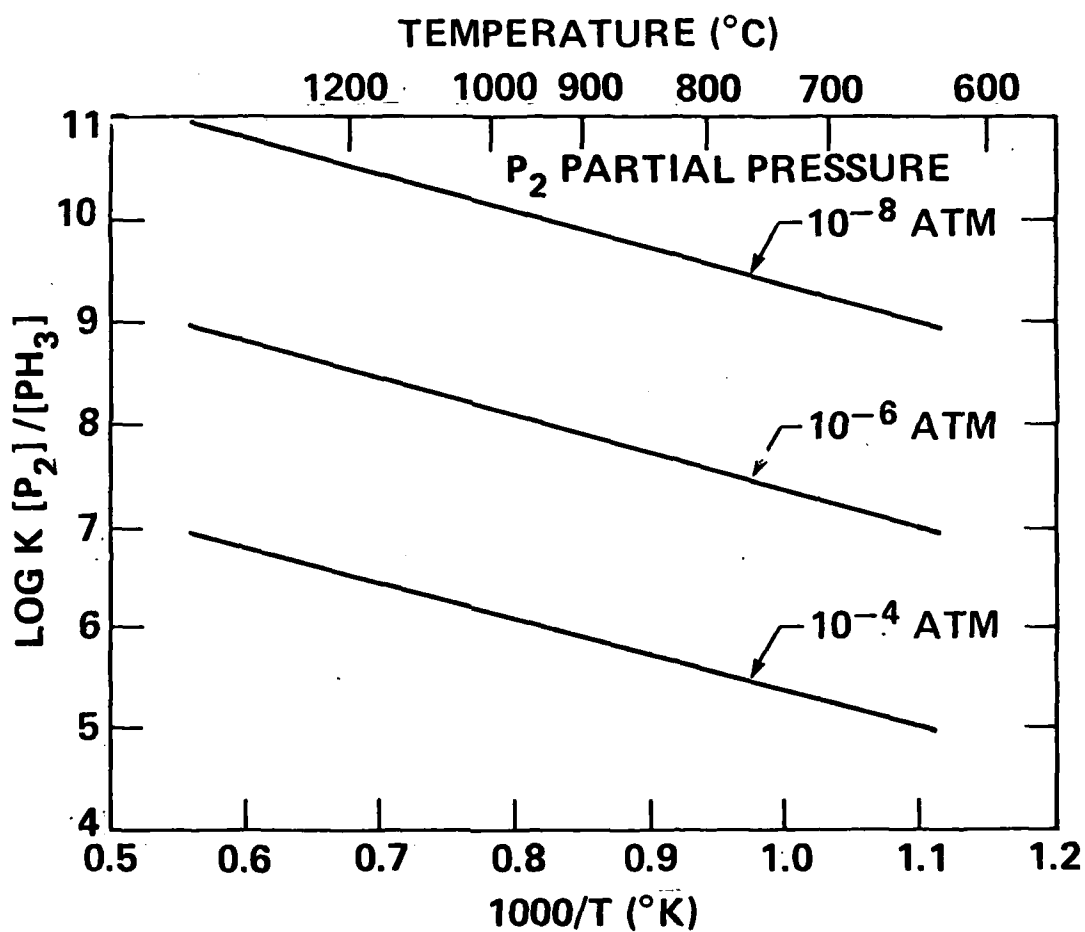


Fig. 3 $[\text{P}_2]/[\text{P}_4]$ ratio versus inverse temperature at three P_2 partial pressures. The ratio is much greater than one at all the given temperatures and partial pressures.



III. EXPERIMENTAL

A. System Design for Cracking Experiments

A ultra-high vacuum station was assembled for the PH_3 cracking experiments and obtaining experience with the handling of PH_3 and phosphorus in vacuum. Figure 4 shows the schematic diagram of the vacuum station during the first series of cracking experiments. The system has two sorption pumps, a titanium sublimation pump (TSP) with a condenser, one 140 l/s ion pump, and one liquid-nitrogen cooling panel (not shown). Pump oil is excluded from the system, thus eliminating hydrocarbon contamination. An ion gauge is used to measure the system pressure and indicate roughly the flow rates. The TSP is water (or LN_2) cooled in expectation of pumping the hydrogen from cracked PH_3 . The millitorr gauge was installed for monitoring the pressure increase of white phosphorus at room temperature. A LN_2 cryoshroud is also available in the vacuum station for controlling the white phosphorus pressure.

The vacuum system also has a nitrogen line to backfill and purge the chamber when it is necessary to expose the chamber to atmosphere. Also, the nitrogen line is directly connected to the source line for purging the regulator and the bubblers.

B. Safety Aspects of Using Phosphine

The toxicity of PH_3 in these experiments presented an immediate health concern. The time-weighted average limit set by OSHA is 0.3 ppm/8 hours, the low toxic concentration level is 8 ppm/hour, and the odor threshold is about 2 ppm [5-6]. The apparatus was enclosed as far as practical in a hood, with forced ventilation around the entire vacuum station and gas-handling system. The pumps were also housed in this enclosure. The forced ventilation exhausted through the main building scrubber unit. The enclosure provided a protective barrier

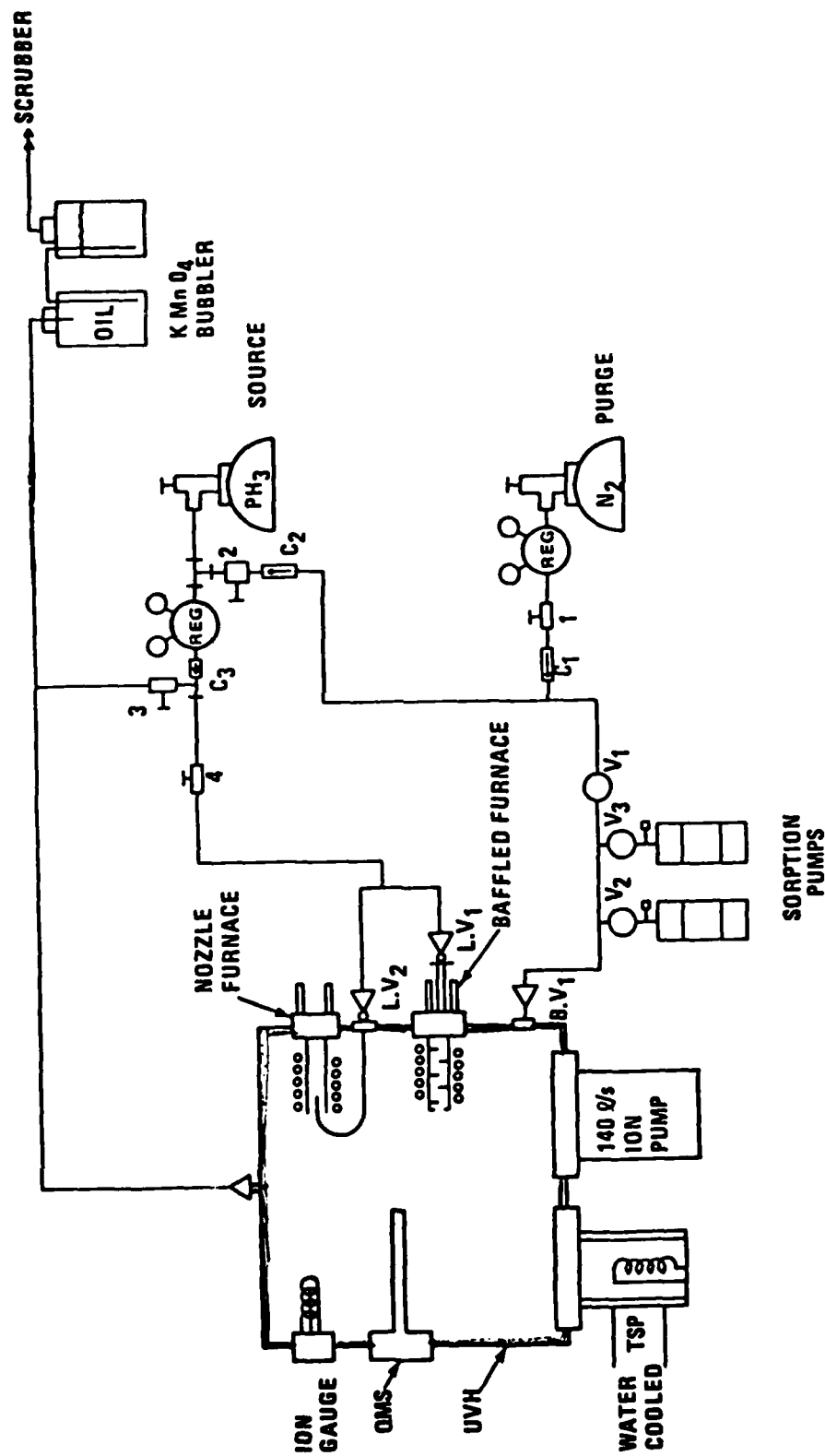


Fig. 4 Sketch of ultra-high vacuum station and gas-handling system used in the furnace cracking experiments. The nozzle furnace and fixed baffle furnace are shown.



between the operating personnel and the gas in case of an accidental rupture. Special attention was applied to the design of the exhaust and purging systems in order to minimize the amount of PH_3 which went into the scrubber unit. The following options were considered:

1. Dilution

Dilution with air is a very simple method, relying on the PH_3 to decompose naturally into its elements in due course. If this method is chosen, the exhaust of the vent must be carefully located with respect to any residential areas or air intakes of office buildings. Since our laboratory is located in a built-up area, this method was immediately ruled out.

2. Thermal Decomposition

High-temperature furnaces such as flare stacks or atmospheric pressure crackers decompose the PH_3 into less toxic substances, an oxide of phosphorus and hydrogen. This method is suitable for handling large volumes of the gas quickly, but was rejected because of the relatively large amounts of hardware required.

3. Activated Charcoal

Activated charcoal impregnated with $\text{K}_2\text{Cr}_2\text{O}_7$, Ag_2CrO_4 , or a proprietary metallic can be used to adsorb gas. Fifty-five gallon drums of activated charcoal are commercially available from Calgon Corporation under the trade name Ventsorb. The cost was about \$1000 per drum, which contains 150 pounds of charcoal. If we assume that the charcoal adsorbs 10% by weight of the PH_3 , the remaining charcoal adsorbs other gas constituents, then 15 pounds of PH_3 could be disposed of in the drum. This adsorption capacity is suitable for pressurized gas cylinder with an 8" diameter and 27" length which usually



holds 6.6 pounds of PH_3 . Disadvantages of this method are the laboratory space requirements because of the size of 55-gal drums, and the possibility of an accidental desorption occurring if the drum heats up when the vacuum stations are baked out.

4. Bubblers

The bubbler method consists of bubbling the PH_3 through a solution which either reacts with the gas or takes the gas into solution (i.e., NaOCl) and bromine under water (i.e., KMnO_4). The NaOCl was not used because it would be difficult to determine the PH_3 saturation of the solution. The PH_3 forms PBr_3 with the bromine and a phosphorus oxide with the KMnO_4 . The bromine solution was not used because of its extremely corrosive nature, and the requirement of another bubbler stage to neutralize the bromine (i.e., a NaOH and KOH stage). If PBr_3 is similar to AsBr_3 , then the bubbler solution product has a toxicity similar to arsenic.

The PH_3 disposal system used for the experiments was a KMnO_4 bubbler. The original setup was a two-stage bubbler, as shown in Fig. 4, but was later expanded to a three-stage bubbler in the final version. The first stage was simply an empty bottle between the vacuum station and the bottles with the KMnO_4 solution, so as to prevent accidental syphoning of the solution. Six grams of KMnO_4 were dissolved in 200 ml of water and equally divided into two polyethylene bottles, the second and third bubbler stages. The exhaust of the first stage bubbled into the second stage through a 6-mm pyrex tube. The exhaust of the second stage bubbled into the third stage through a gas-dispersion (glass-fritted) tube. The purple KMnO_4 solution turns brown when the solution needs more KMnO_4 . A set of procedures (see Appendix A), was written to cover the general and emergency for operating personnel.



C. Cracking Furnaces

Initially, two different types of crackers were constructed -- a nozzle furnace and a fixed-baffle furnace. After comparing the results from both furnaces, the efforts focused on the development of a different design of baffle furnace because it yielded a higher cracking efficiency than the nozzle furnace. The details of each furnace are given below.

The motivation for trying a nozzle furnace was its simplicity. As sketched in Fig. 4, the nozzle furnace consists of a nozzle directing the gas flow from a leak valve into a furnace -- in this case, a MBE furnace with a pyrolytic boron nitride crucible. The model for cracking with a nozzle was to dissociate the PH_3 molecule on its one-time contact with the heat crucible surface.

A fixed-baffle furnace was constructed with molybdenum, tantalum, braze filler and alumina parts. The baffling was to increase the number of collisions that a PH_3 molecule had with a hot wall, thus simulating the effects of a long furnace. The drawbacks with the fixed-baffle furnace were that it had no thermocouple and a current-limit of 3 amps.

The next baffle furnace was made with a higher current-limit to investigate the anomalies found with the fixed-baffle furnace. This design features a replaceable cartridge; cartridges of varying numbers of baffles and materials could be tested on the same furnace. A sketch of the cartridge furnace is shown in Fig. 5. The supports, heat shields, and windings are tantalum and the winding insulators are pyrolytic boron nitride. The support material is tantalum sheet, 0.051-mm thick, wrapped on a mandrel and spot welded into a cylindrical form. The front, back, and cylindrical heat shields consist of 5 layers of .025-mm thick tantalum foil and a final layer of .254-mm thick tantalum sheet. About 2.54-m of 0.635-mm diameter tantalum wire was used in the windings.

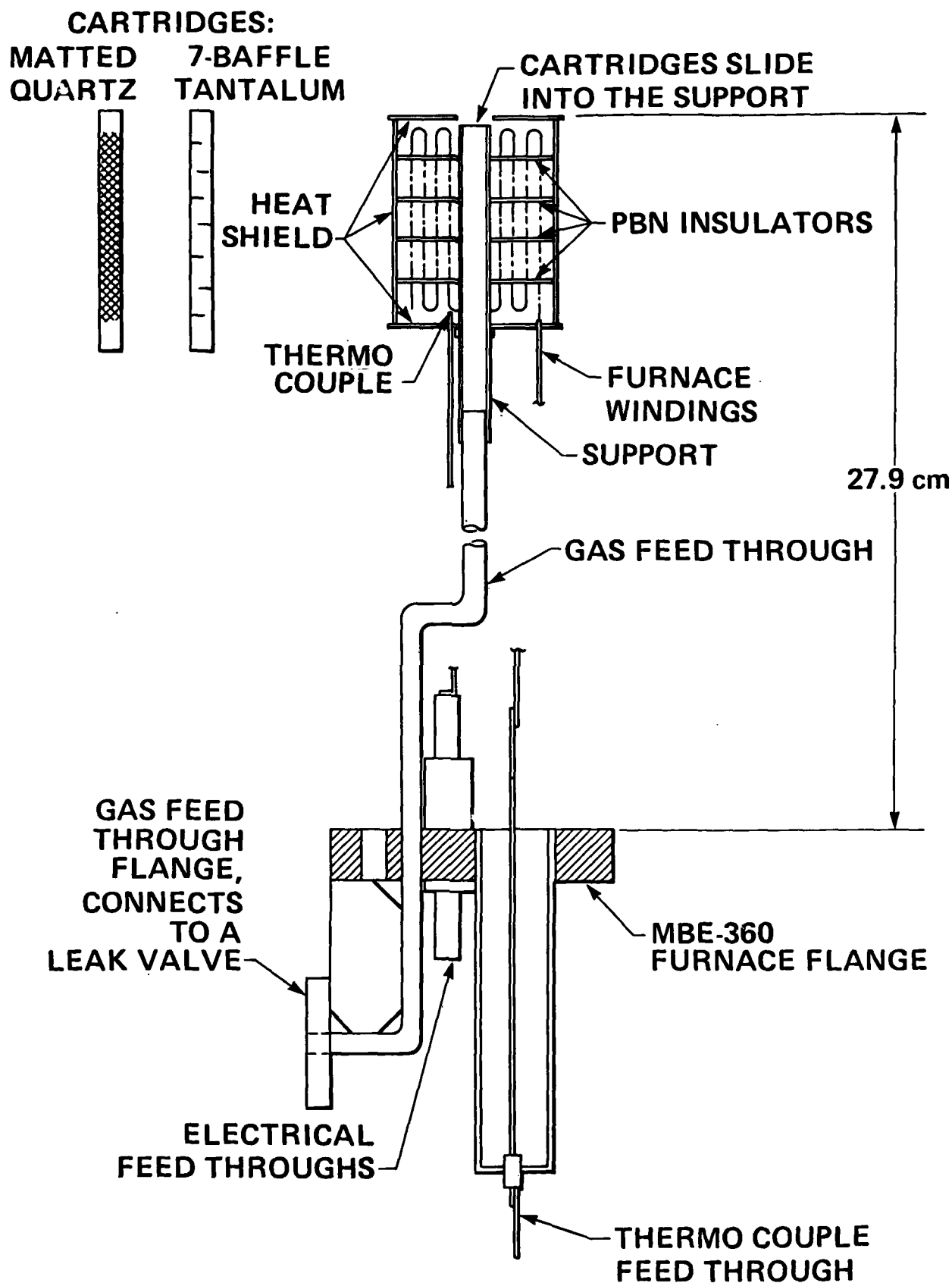


Fig. 5 Sketch of PH_3 cartridge furnace, 7-baffle tantalum cartridge, and matted quartz-filled cartridge.



The furnace hot zone dimensions in the support are 4-cm in length by 0.6-cm diameter. The pyrolytic boron nitride insulators are 3.18-cm diameter, 0.635-mm thick discs. The furnace is mounted on a stainless steel gas feedthrough, which leads to a leak valve. A tungsten-rhenium thermocouple contacts the inside of the back heat shield, near the support. The power, thermocouple, and gas feedthroughs are all mounted on a 6.98-cm conflat flange. The overall dimensions of the cracker assembly are 27.9-cm in length from the conflat flange knife edge to the furnace orifice, and 3.36-cm in diameter.

A cartridge could be inserted into the hot zone of the furnace such that the PH_3 gas molecules equilibrate to a high temperature, surrounded by the cartridge material. Cartridges of tantalum were made with zero, 2, and 7 baffles. A quartz zero-baffle cartridge, a 7-baffle cartridge, and a quartz cartridge filled with matted quartz fibers were also constructed.

The furnace and cartridges were rinsed with solvents in the order: TCE, acetone, and methanol. The furnace was vacuum fired at 1000°C overnight before beginning the PH_3 testing. The cartridges were vacuum fired individually prior to their use in a test run. The temperature was controlled manually with an isolated variac transformer. The furnace temperature was easily controlled, especially at temperatures above 500°C. The power required to reach 1170°C was 210 watts.

D. Experimental Conditions

The cracking efficiency is defined by the difference between the PH_3 partial pressure values at room temperature and the operating temperature, and then divided by the former value. The cracking efficiency increased by only a factor of two as the flow rate increased by about two orders of magnitude, corresponding to a change in background pres-



sure from 10^{-7} Torr to 10^{-5} Torr. The thermodynamic situation predicts a decrease in efficiency because, according to the reaction $P + 3H \rightleftharpoons PH_3$, additional PH_3 will lead to a slowing of the rate of increase of total pressure. What may be occurring in the furnace hot zone is that as the flow rate increases, the gas transport mechanism becomes less molecular and more viscous. As the flow becomes viscous, the gas can heat up conductively, as well as radiatively. The cracking efficiency then increases because the thermal heating of the gas becomes more effective. Nevertheless, the cracking efficiency changes very slowly with flow rate. Accordingly, the flow rate was kept constant during the PH_3 cracking experiments, to stabilize the background pressure at about 1×10^{-6} Torr.

A quadrupole mass spectrometer was used to measure the partial pressures of the species emitted from the furnace. Spectra from 2 amu to 270 amu were taken before and after the introduction of 5-nines pure PH_3 into the vacuum system. These two spectra, reproduced in Fig. 6 on a log-log scale, showed:

1. water as the major impurity of the vacuum station;
2. inert gases and hydrogen as the major impurities of the PH_3 source;
3. the formation of P_2As_2 , P_3As and PAs_3 by-products (the vacuum station had previously been used for arsenic experiments);
4. the cracking pattern of PH_3 into phosphorus tetramer, dimer and monomer species by the quadrupole mass spectrometer probe was found to be constant for all furnaces when the cracker was off.

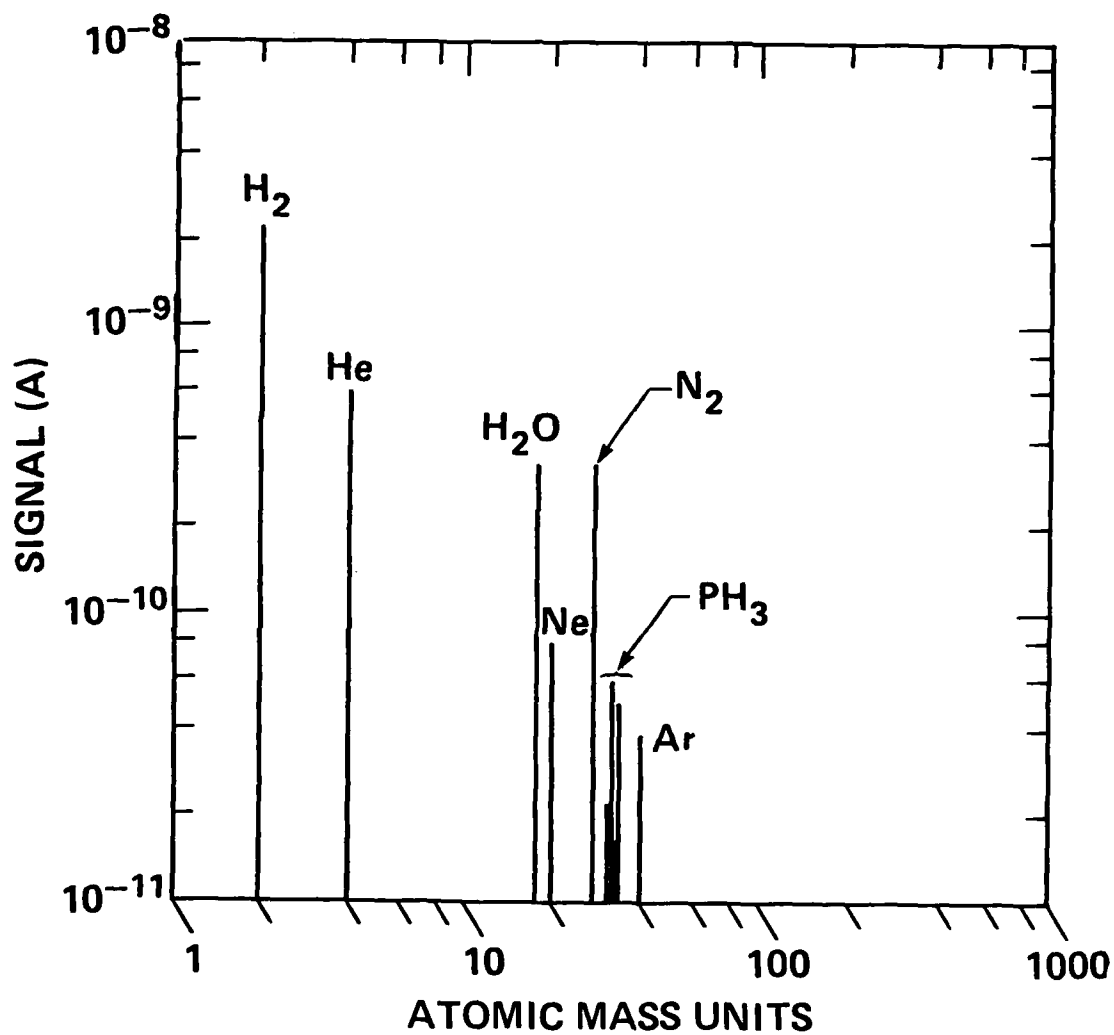
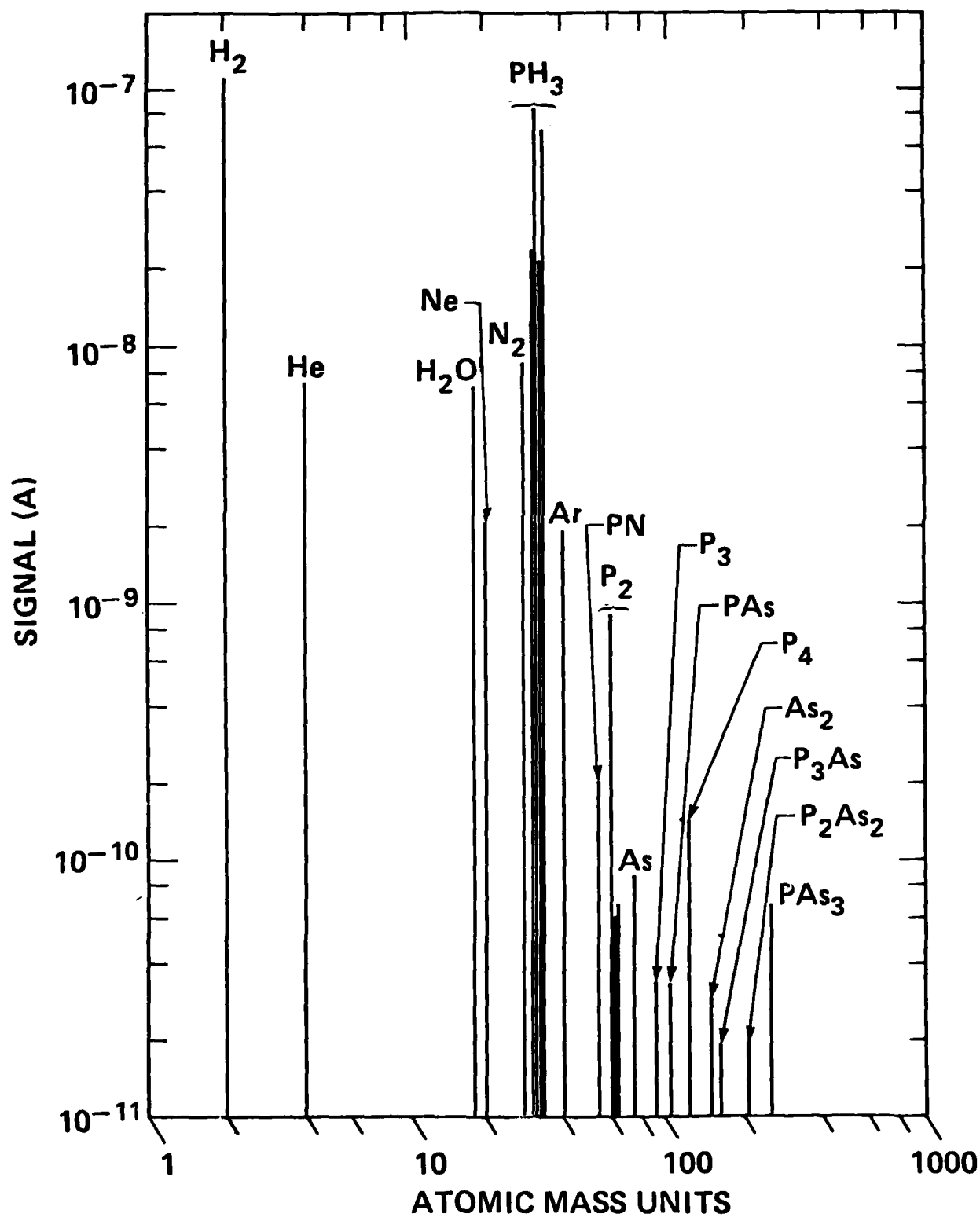


Fig. 6a Quadrupole mass spectrum of the background gases before the introduction of PH_3 into the vacuum station used for the cracking tests.

Fig. 6b Quadrupole mass spectrum of background gases after introduction of PH_3 into the vacuum station used for cracking tests.





The measured phosphorus concentrations with increasing temperatures were adjusted to account for the probe contributions.

One interesting note on item number three is that when the furnace temperature increased, the concentration of by-products varied according to the P_2 concentration and not the PH_3 concentration. It appears that P_2 reacts more readily with residual As in the system than PH_3 to form phosphorus-arsenic compounds.

The results of the cracking experiments are discussed in Section IV below.

E. System for Growth Experiments

After the cracking experiments were complete, a Varian MBE-360 system [7] was modified to handle PH_3 . The vacsorb exhausts were vented into the house scrubber system. The PH_3 gas tank and tubing up to the leak valve on the MBE-360 were enclosed in a ventilated housing and large-diameter pipe. A separate vacsorb in the ventilated housing was used specifically for the PH_3 regulator and tubing. The quartz 7-baffle cartridge furnace was installed into the MBE-360. This system had no water cooling available for the Ti-ball pump and so three fans were used to circulate air around the Ti-ball sump instead. This method kept the sump relatively cool when the Ti-ball sublimation rate was < 0.05 mm/hr. However, this speed appeared to be too slow to reduce the hydrogen load on the 400 /s ion pump of the growth chamber. With a pressure during growth at 2×10^{-5} Torr, ion pump instability occurred around 4 hours into the growth. Air cooling the ion pump proved more effective than on the Ti-ball pump. The air-cooled ion pump remained stable throughout our longest growth run (eight hours). Additional pumping during growth was done by the LN_2 cryo-paneling around the growth chamber.



Liquid-encapsulated Czochralski-grown (LEC) InP substrates of (100) orientation and chromium doping were used. The substrates were chemo-mechanically polished in a hydrobromic acid solution. An initial surface preparation consisted of degreasing the substrate in warm TCE, acetone, methanol, and IPA baths with ultrasonic action; next followed a de-oxidizing of the surface by stagnant immersion in sulfuric acid for 5 minutes and in a 1:14 solution (H_2O_2 , H_2O , H_2SO_4) for 2 minutes; and then a re-oxidizing of the surface by heating in H_2O for 5 minutes after rinsing off the 1:14 solution. The substrates were bonded onto molybdenum heater blocks with indium, and introduced into the MBE-360 system through the load-lock. The substrates were outgassed in a preparation chamber at a temperature of 240°C for 15 minutes. The final in-situ cleaning step was done under a phosphorus flux in the growth chamber, in which the temperature was raised to and maintained at 450°C for at least 2 minutes before resetting the controller to the growth temperature.

The upper limits on the P_2 flux which could be used was set by the co-generated H_2 pressure of 2×10^{-5} . This limit on the P_2 flux, normally monitored as $\sim 4 \times 10^{-8}$ Torr from the QMS probe, sets the limit on the growth rates to $0.4 \mu\text{m/hr}$. The initial InP-MBE growths with the cracker was to check the uniformity of the epitaxy grown on GaAs substrate. Once the position was found, the growth rate was calibrated, and the substrate temperature was increased from 240°C to 450°C .

Unintentionally-doped InP layers were grown 1.4 microns thick at a ~ 0.4 micron/hour growth rate. Van der Pauw measurements were made at 300°K and 77°K with a 4.1 Kgauss magnet. An In-Sn alloy was used at the contacts for the van der Pauw measurements. The PL spectra reported below were made at 77°K with an argon laser emitting at 5145 \AA .



IV. RESULTS AND DISCUSSION

This section consists of two parts. The first part will describe the development of the cracker furnace, in which three furnaces were made and tested. They were a nozzle furnace, a fixed-baffle furnace and a cartridge furnace. The key was to develop, at lower temperatures, a high cracking efficiency defined as the difference of PH_3 partial pressures between room temperature (P°) and the operating temperature pressure (P) divided by the room-temperature pressure, $[P^\circ - P]/P^\circ$. In the second part of the section, the properties of the growths are given, (Van der Pauw measurements and photoluminescence spectra).

A. Cracker Furnace

The first phase of developing a cracker involved comparing the results from the two different types of furnaces, a nozzle furnace and a fixed-baffle furnace. The results are given respectively in Figs. 7 and 8, where the partial pressures of PH_3 , P_2 and P_4 are plotted as a function of temperature (nozzle furnace) or current in the furnace winding (fixed-baffle furnace).

The nozzle furnace shows a 38% cracking efficiency at a temperature of 1300°C , according to Fig. 7. What is not observed here, but is found with the other furnaces, is a corresponding increase in the P_4 or P_2 concentrations. The increase in the P_2 concentration occurs very gradually over the entire temperature range. The increase of the P_4 concentration saturates at 500°C .

The results of the fixed-baffle furnace in Fig. 8 were more encouraging, although somewhat perplexing. The fixed-baffle cracking efficiency was over 90% at a 2.9-amp circuit setting. A temperature of $\sim 720^\circ\text{C}$ was read from a thermocouple placed at the furnace orifice

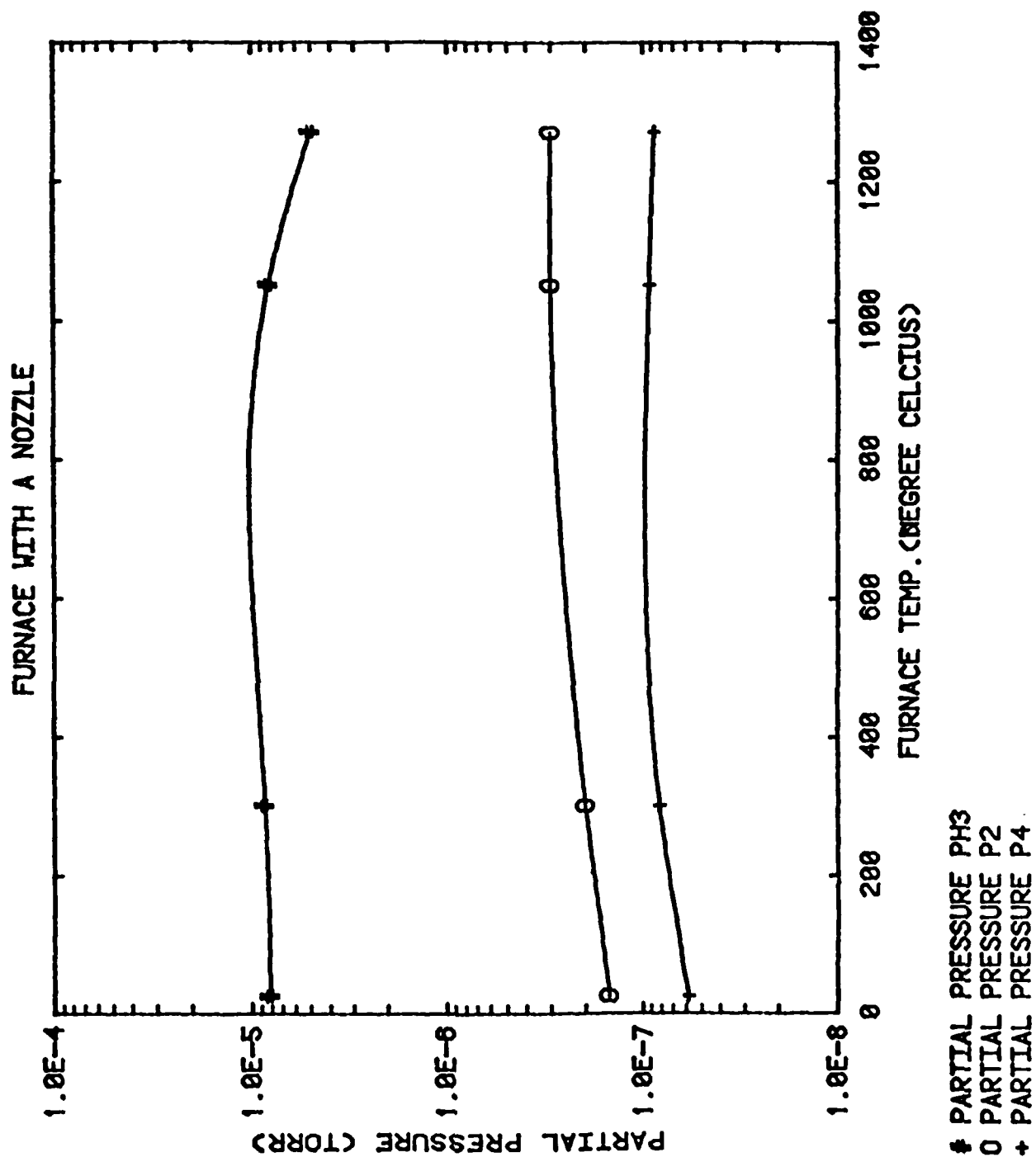


Fig. 7 Partial pressure of PH_3 , P_2 and P_4 versus temperature of the nozzle furnace. The PH_3 curve shows a 38% cracking efficiency at 1300°C .

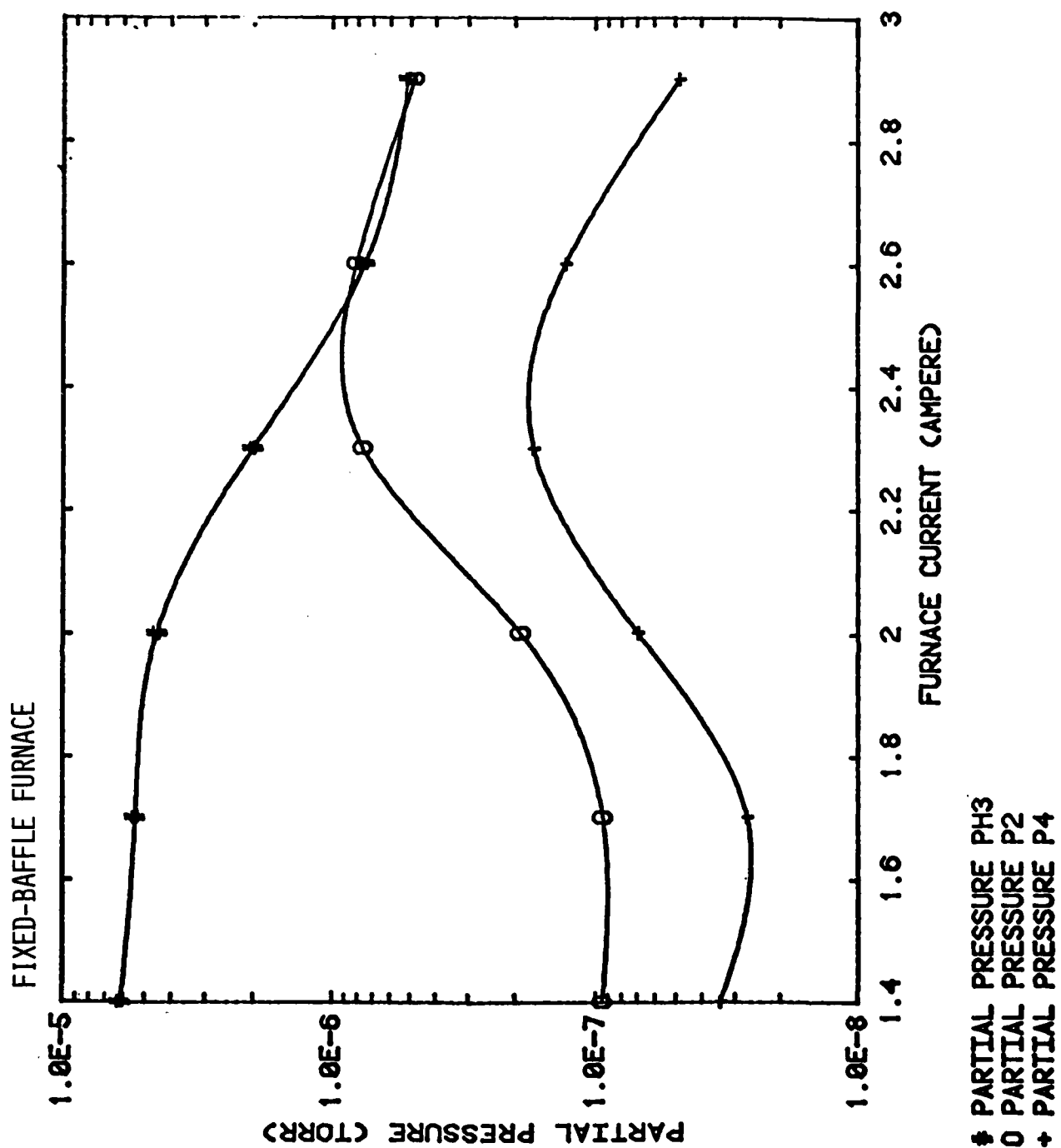


Fig. 8 Partial pressure of PH₃, P₂ and P₄ versus current in the fixed-baffle furnace winding. The PH₃ curve shows a 90% cracking efficiency at 2.9 amp.



at this current. The questions arise because of the peaking in the P_2 and P_4 concentrations which occur above 2.4 amps. What was expected was a continuous increase of P_2 plus P_4 concentrations until the PH_3 was completely dissociated. One of two things may be occurring in the fixed-baffle furnace -- insufficient heating to cause a thorough cracking of PH_3 , or a reaction of PH_3 with the furnace material such as the braze, molybdenum or tantalum. To conduct a more detailed investigation, the cartridge furnace was designed with a higher power density, a thermocouple on the back end of the furnace, and a simple procedure to vary the number of baffles and material in the hot zone through the use of cartridges.

The results of the 7-baffle tantalum cartridge are shown in Fig. 9. The signal currents for H_2 , PH_3 , P , P_2 and P_3 are plotted as a function of the furnace temperature. Note the following trends as the furnace temperature increases:

- (1) The cracking efficiency of PH_3 increases between $\sim 200^\circ C$ and $600^\circ C$ and then decreases from $600^\circ C$ to $1070^\circ C$.
- (2) The phosphorus monomer, dimer, and tetramer concentrations fall and rise together;
- (3) The phosphorus concentrations peak at $400^\circ C$, dip to a low value at $\sim 700^\circ C$, and then continue to rise with temperature from $700^\circ C$ upwards.

We now believe that various reactions of PH_3 with tantalum cause these anomalous peaks and dips in the phosphorus concentrations.

A confirmation came in the comparison of the tantalum zero-baffle, 2-baffle, and 7-baffle results, as shown in Fig. 10. The curves represent the dimer intensities normalized to the PH_3 intensities plotted

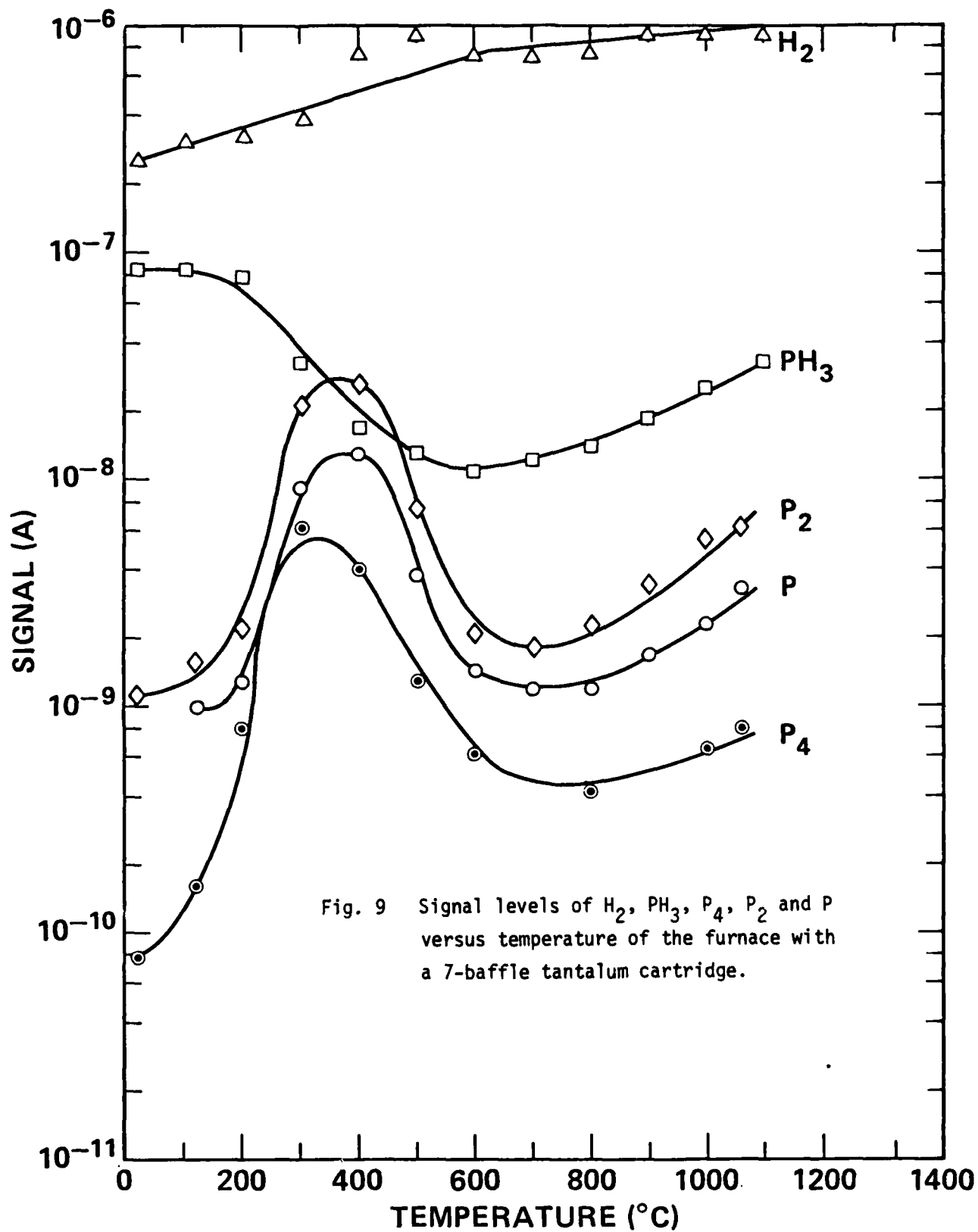


Fig. 9 Signal levels of H_2 , PH_3 , P_4 , P_2 and P versus temperature of the furnace with a 7-baffle tantalum cartridge.

7-BAFFLE TANTALUM CARTRIDGE

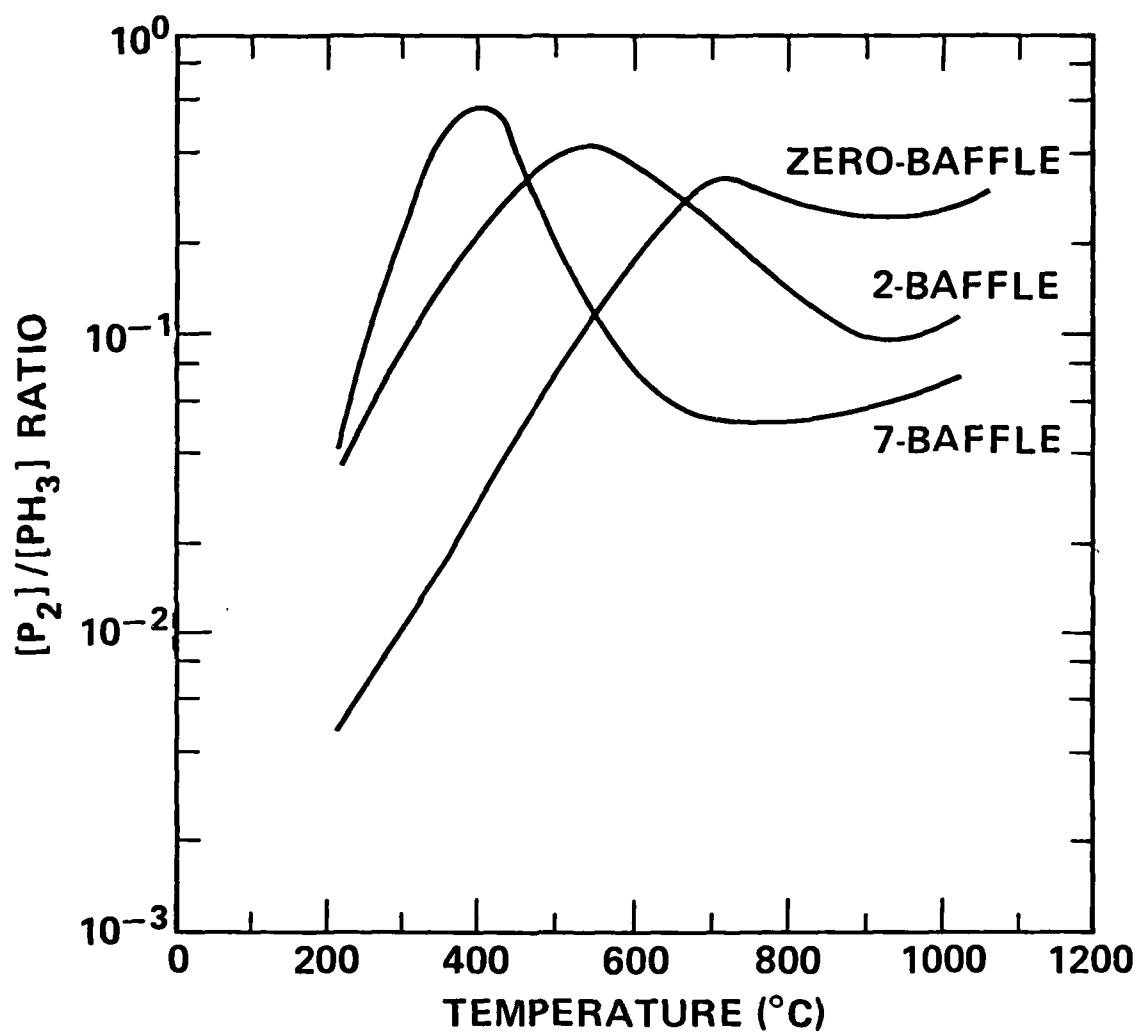


Fig. 10 P_2 partial pressure normalized to PH_3 partial pressure and plotted versus temperature. The results are obtained from the cracker furnace using the zero-baffle, 2-baffle and 7-baffle tantalum cartridge.



versus furnace temperatures. As the number of baffles declines (the surface area of tantalum decreases), two observations are made. First, the maxima of the peaks decrease, and they occur at higher temperatures. Second, the minima of the dips increase and move to higher temperatures. The less tantalum there is in the cartridge, the less severe the peaks and valleys and the more energy required to produce the peaks and dips.

The PH_3 can react with tantalum in two ways. First, the tantalum-hydrogen binary phase diagram shows that a tantalum hydride forms in the temperature range of 100-600°C [8]. If this reaction occurs in the furnace, the formation of tantalum hydride could act as a catalyst in cracking PH_3 by stripping away the hydrogen from the PH_3 molecule, increasing the phosphorus concentrations at the lower temperatures. Second, tantalum phosphide compounds TaP_n , $n = 1$ to 2, exist at 816°C, 0.22 Torr, in the temperature range where the dips occur [9]. Therefore, it is likely that PH_3 forms a tantalum phosphide with the tantalum cartridge before it is cracked into phosphorus. The slight rise in the P_2/PH_3 ratio at high temperatures may be caused by the dissociation of TaP_n , $n = 1$ to 2, to a TaP compound, found to occur above 900°C [10].

Further proof that the tantalum phosphide compounds are indeed formed is derived from electron spectroscopy for chemical analysis (ESCA) performed on a tantalum cartridge used in these experiments. In Fig. 11, the binding energies of the valence electrons for tantalum and phosphorus are compared with their elemental values. The binding energy of phosphorus is reduced by 0.6 eV, indicative of what occurs when phosphorus bonds to less electronegative materials like Mn, Ga, and B. The binding energy of tantalum is increased by 1.3 eV, indicative of what occurs when tantalum binds to a more electronegative material like carbon. Since phosphorus is more electronegative than tantalum, the binding energy shifts are evidence that tantalum is bonding with phosphorus. No simple stoichiometry was found, but the average compound was tantalum rich.

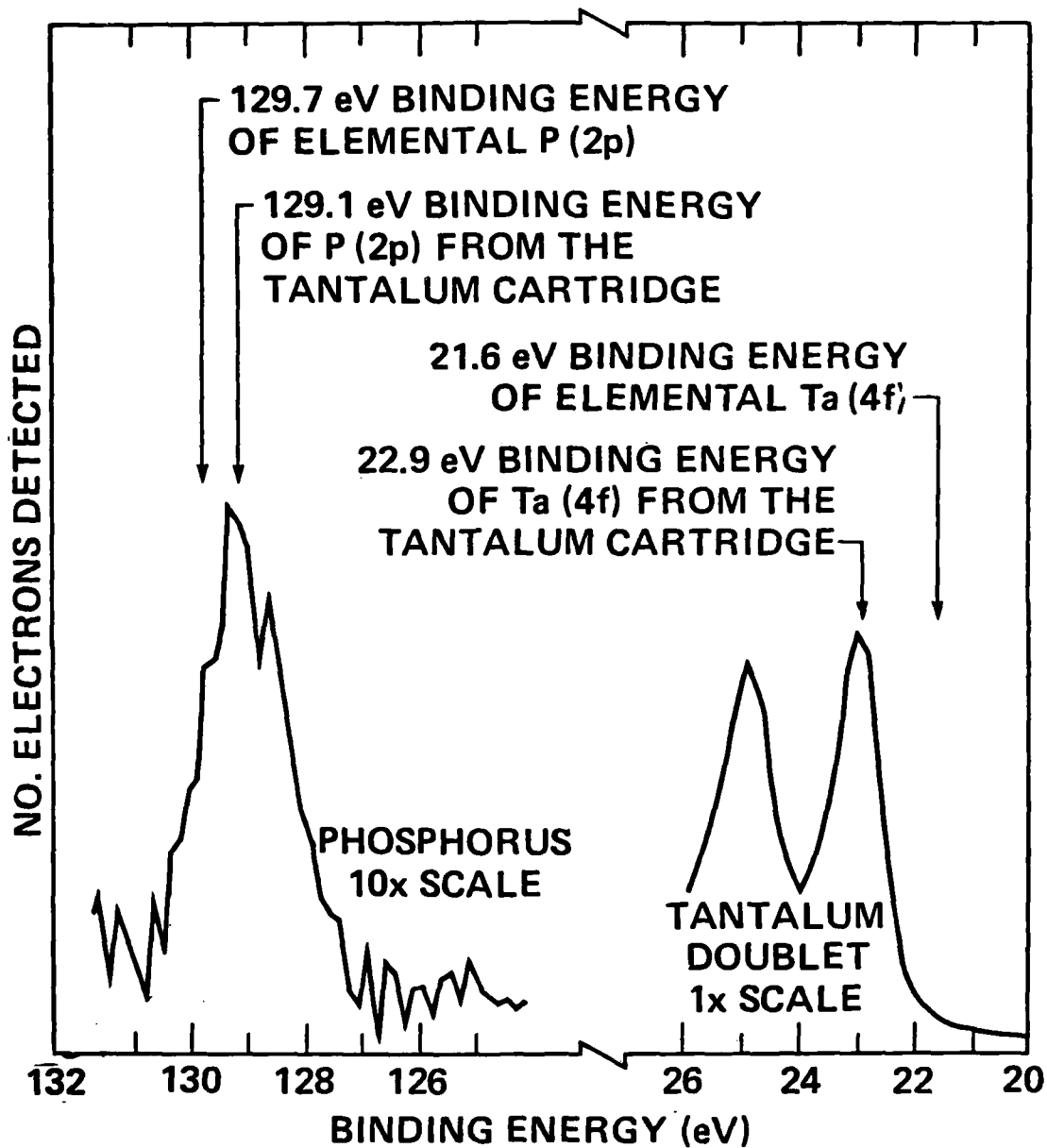


Fig. 11 ESCA spectrum of a tantalum cartridge used for cracking PH_3 . Binding energy for the phosphorus 2p electron is reduced and the binding energy for the tantalum 4f electron is decreased, indication formation of tantalum phosphide compounds. The spectrum for the tantalum 4f electronic level shows as a doublet, caused by the $\pm 1/2$ electronic spin components.



Since there is evidence of PH_3 reactions with tantalum, further cracking experiments were performed on the two quartz cartridges. The results of the zero-baffle quartz cartridge and the cartridge filled with matted quartz are given in Figs. 12 and 13, respectively, for comparison with Fig. 9. The curves are the signal currents of H_2 , PH_3 , P_4 , P_2 and P plotted as a function of the furnace temperature. The peaks and dips associated with tantalum cartridges are not observed when the quartz cartridges are utilized.

For the zero-baffle quartz, the cracking of PH_3 occurs at about 550°C , as seen by the break in PH_3 signal into a steeper slope and the rise of the phosphorus signals. The phosphorus P and P_2 signals saturate at 1000°C , which indicates that the furnace has reached its maximum cracking efficiency. The cracking efficiency of the zero-baffle quartz cartridge cracker is 77%, defined by the difference of PH_3 partial pressure at room temperature and its lowest value over the initial PH_3 partial pressure.

The cracking characteristics of the furnace improve when the matted quartz-filled cartridge is used instead of the zero-baffle quartz cartridge. The cracking efficiency is greater than 90% and the temperature at which the phosphorus signals saturate is lowered to 400°C .

It is clear from Fig. 13 is that the PH_3 signal is still decreasing in spite of the fact that the phosphorus signals have already leveled off. This is attributed to the slower pumping speed that the ion pump has for PH_3 than for phosphorus. A difference in pumping speeds was found when the pump was turned off and then observing a rise in the PH_3 signal by several orders of magnitude while the phosphorus signals remained constant on the quadrupole mass spectrometer. In an earlier test with the fixed-baffle furnace, one cracking experiment was per-

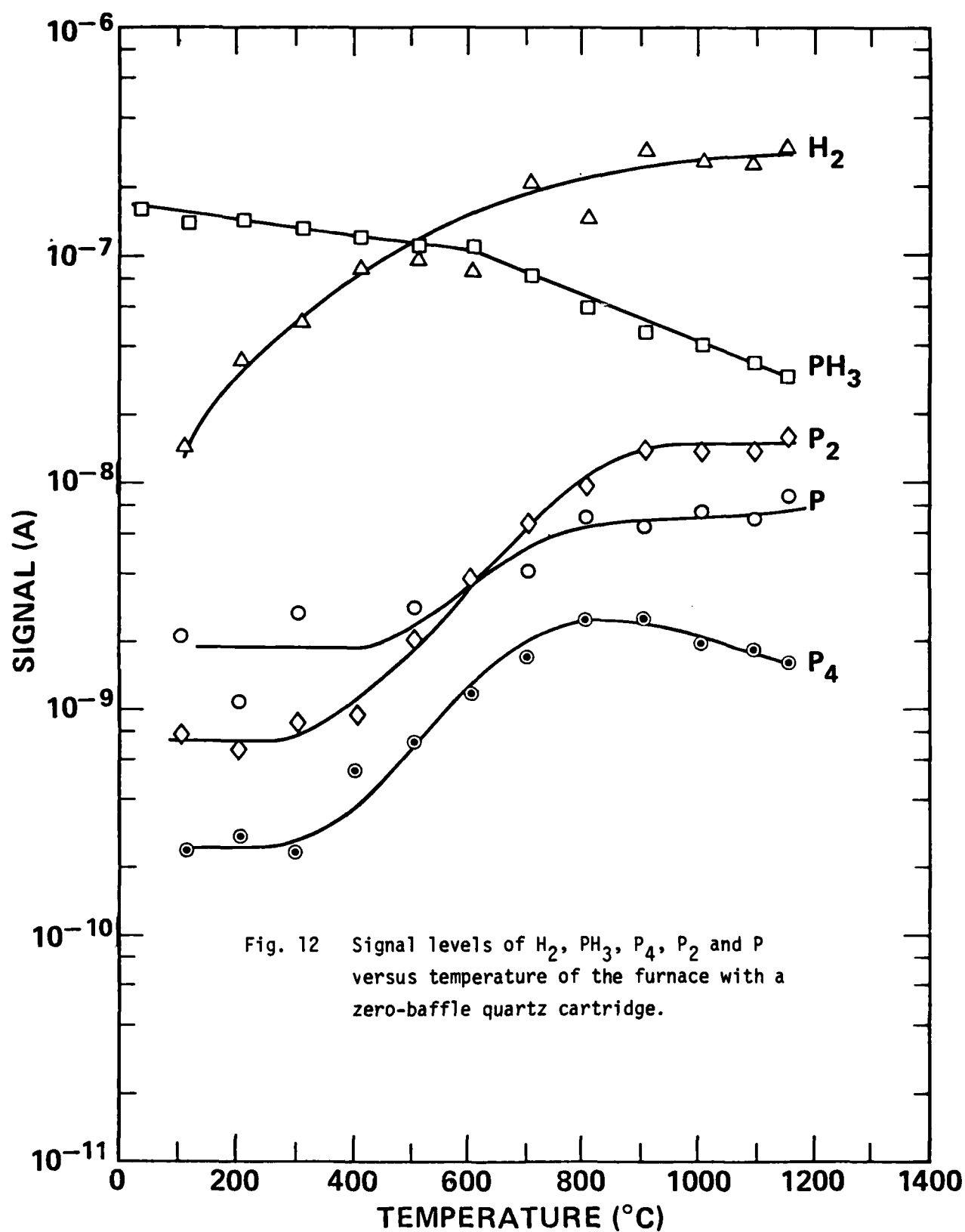
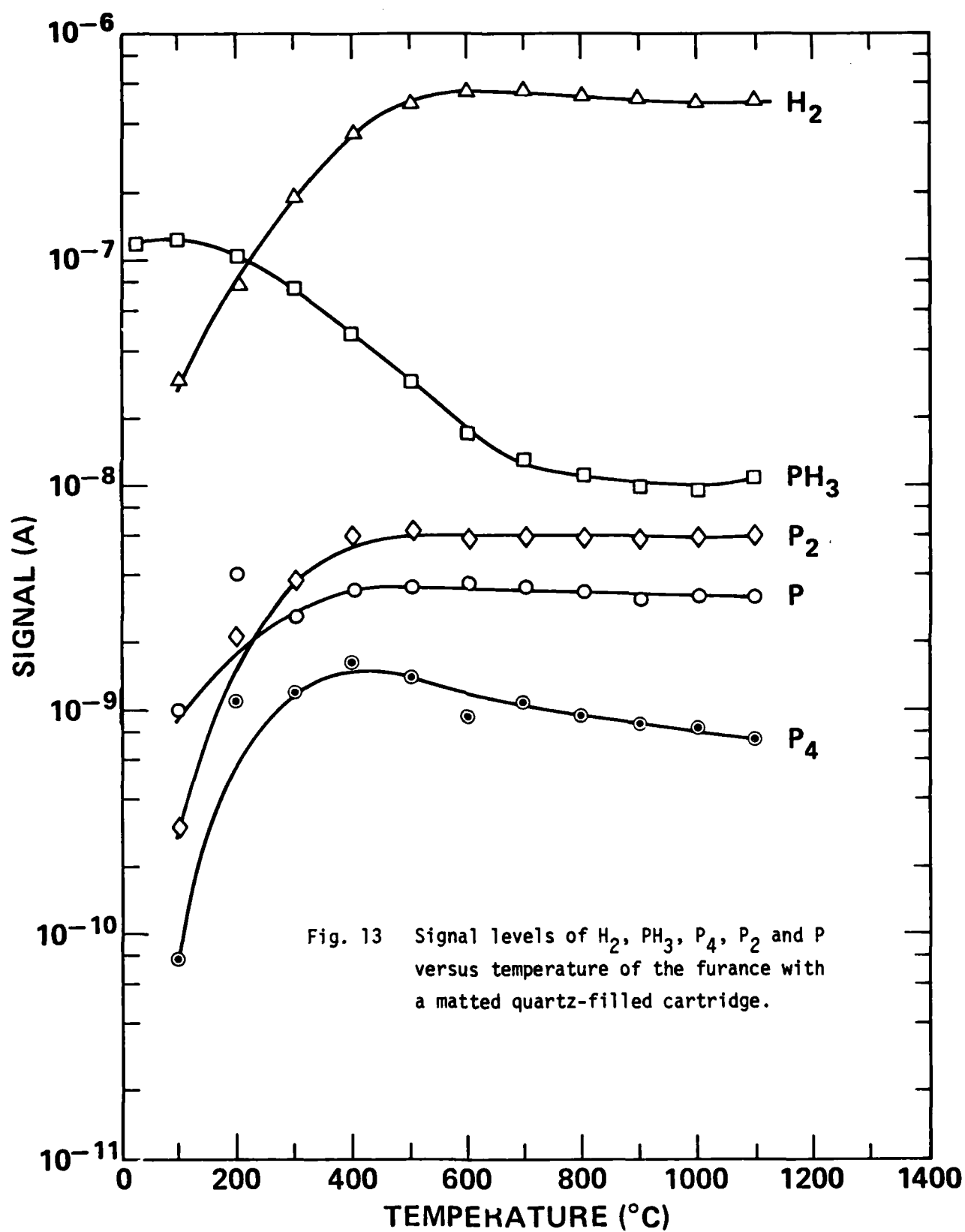


Fig. 12 Signal levels of H_2 , PH_3 , P_4 , P_2 and P versus temperature of the furnace with a zero-baffle quartz cartridge.

ZERO-BAFFLE QUARTZ CARTRIDGE



**MATTED QUARTZ-FILLED QUARTZ
CARTRIDGE**



formed while cooling the furnace from a high temperature and another while heating up the furnace from room temperature. The PH_3 concentrations showed a hysteresis effect, reproduced in Fig. 14, plotted against the temperature at the orifice. The lower PH_3 signals at a given temperature belonged to the "cooling" experiment. The cracking experiment done while cooling the furnace converted more of the PH_3 into phosphorus initially, and so the ion pump could maintain a lower background PH_3 pressure to lower temperatures. The cracking experiment done while increasing the temperature allows the partial pressure of PH_3 to rise in the background, which in turn leads to a higher PH_3 .

Several comments can be made from these curves in light of thermodynamics. According to Fig. 1, the P partial pressure should be orders of magnitude lower than the P_2 partial pressure. However, Figs. 9, 12, and 13 show a P signal only slightly lower than the P_2 signal. The fact that the P signal follows closely that of P_2 in the entire temperature range leads us to believe that the 31-amu peak on the mass spectrum, which corresponds to the atomic mass of P, is that of doubly-ionized P_2 , and that very little P is generated.

Also, according to Figs. 1 and 2, the P_2 partial pressure should always be greater than the P_4 partial pressure for temperatures greater than -800°C and for P_2 greater than 10^{-4} atm. However, the experimental results do not change as predicted by the equilibrium curve in Fig. 2, indicating that the species in the furnace are not in equilibrium.

Another point of divergence between the experimental and theoretical results concerns the PH_3 partial pressure. According to Fig. 3, PH_3 dissociates into P_2 completely at temperatures above 300°C . Instead, the experimental PH_3 signal decreased by 77% for the zero-baffle quartz cartridge. The addition of matted quartz to the cartridge only

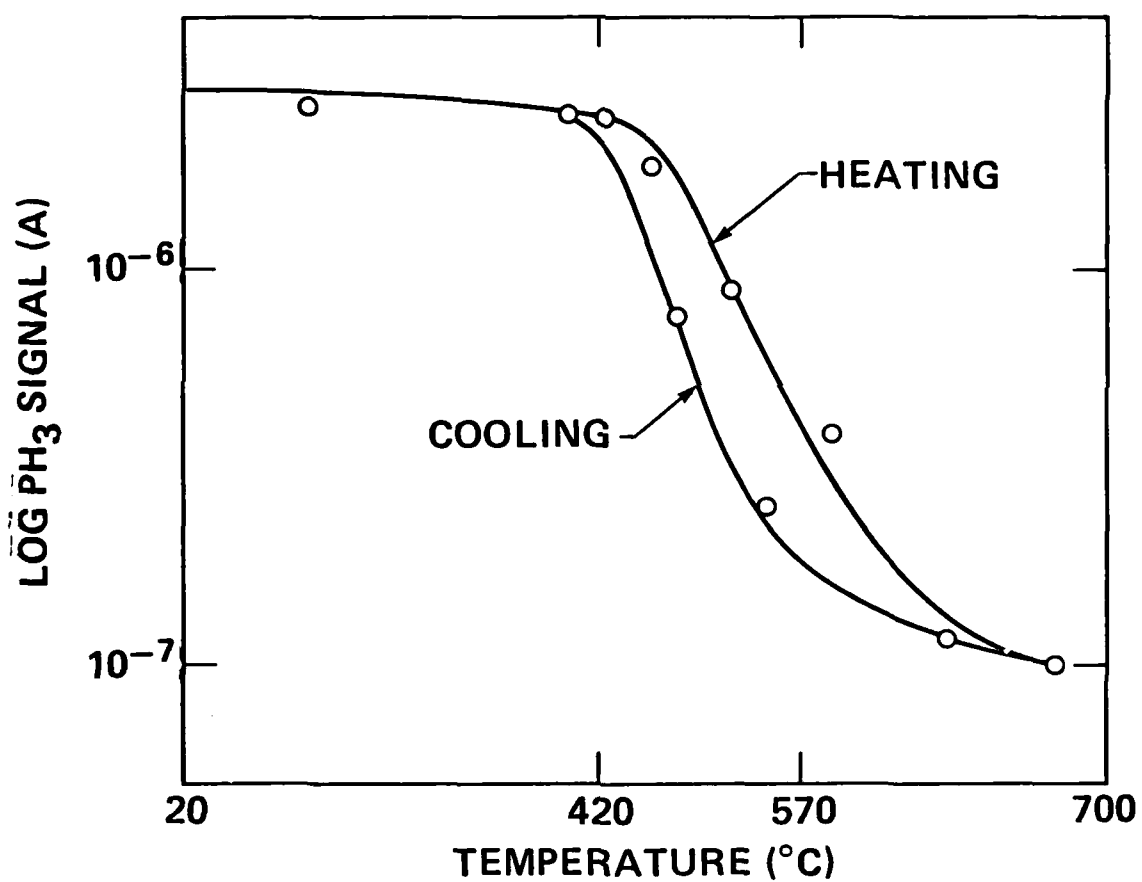


Fig. 14 Hysteresis effect of cracking PH₃ when the experiment begins with a room-temperature furnace and heats up, and when the experiment begins with a hot furnace and cools down.



increased the cracking efficiency to 90%. It may be that the expected decrease in the PH_3 signal is obscured by a high background PH_3 pressure.

B. Materials Characterization

The van der Pauw results are tabulated in Table I for MBE-InP samples #11, #12, #13 and an undoped LEC-InP substrate. The net carrier concentration, unintentionally n-type, decreases and the mobility increases as the substrate temperature increases. McFee et al.³ also found these trends on MBE-InP epitaxies on (111) InP substrates. Whereas McFee et al.³ observed an abrupt change in carrier concentration and mobility at a substrate temperature of about 350°C, we observe a possible inflection between substrate temperatures of 400°C and 450°C, as shown in Fig. 15. At the given substrate temperatures, our unintentional doping concentrations are about 10 times higher than reported in the literature for MBE-InP.^{3,11,12} About 10% of the carrier concentration for our samples freeze out at 77°K, indicating the existence of some deep-level traps. However, the freeze-out of carriers is not as great as that reported by Kawamura et al.¹¹ Sample #13 has a room-temperature compensation ratio of about 2 from Rode's¹³ calculation, and samples #11 and 12 are highly compensated. The compensation ratio compares well with other MBE-InP work. The unintentional doping source may be the phosphine gas-handling system, silicon etched out from the quartz cartridge of the cracking furnace, the occurrence of native crystal defects, or any combination of these.

Figure 16 shows the photoluminescence spectra of an undoped LEC-InP (111) substrate, of sample #12, grown at a substrate temperature of 400°C, and of sample #13 grown at a substrate temperature of 450°C. Sample #11 grown at a substrate temperature of 240°C showed no detectable photoluminescence peak. We note that the near-bandedge peak of 1.41 eV is narrower at the higher substrate temperature. This is due to the decrease in background carrier concentration and corresponds to what

TABLE I: ELECTRICAL AND 77°K OPTICAL PROPERTIES OF MBE-InP

Sample #	T _{ss} °C	N _d -N _a (#/cm ³) 300°K and 77°K	Mobility (cm ² /V-sec) 300°K and 77°K	77°K Bandgap (eV)	Peak Intensities (mV)	Width at 1/2 maximum (meV)	Subpeak-to- Main Peak Ratio
11	240	3.8 x 10 ¹⁸ (3.5 x 10 ¹⁸)	570 (690)	--	0	--	--
12	400	9 x 10 ¹⁷ (8.3 x 10 ¹⁷)	450 (390)	1.412	18	130	--
13	450	1.6 x 10 ¹⁷ (1.2 x 10 ¹⁷)	2410 (2890)	1.409	28	65	0.035
LEC	--	(2 x 10 ¹⁵)	(44,000)	1.410	300	43	.34

461510

K-E 10 X 10 TO THE CENTIMETER
KEUFEL & ESSER CO. MADE IN U.S.A.

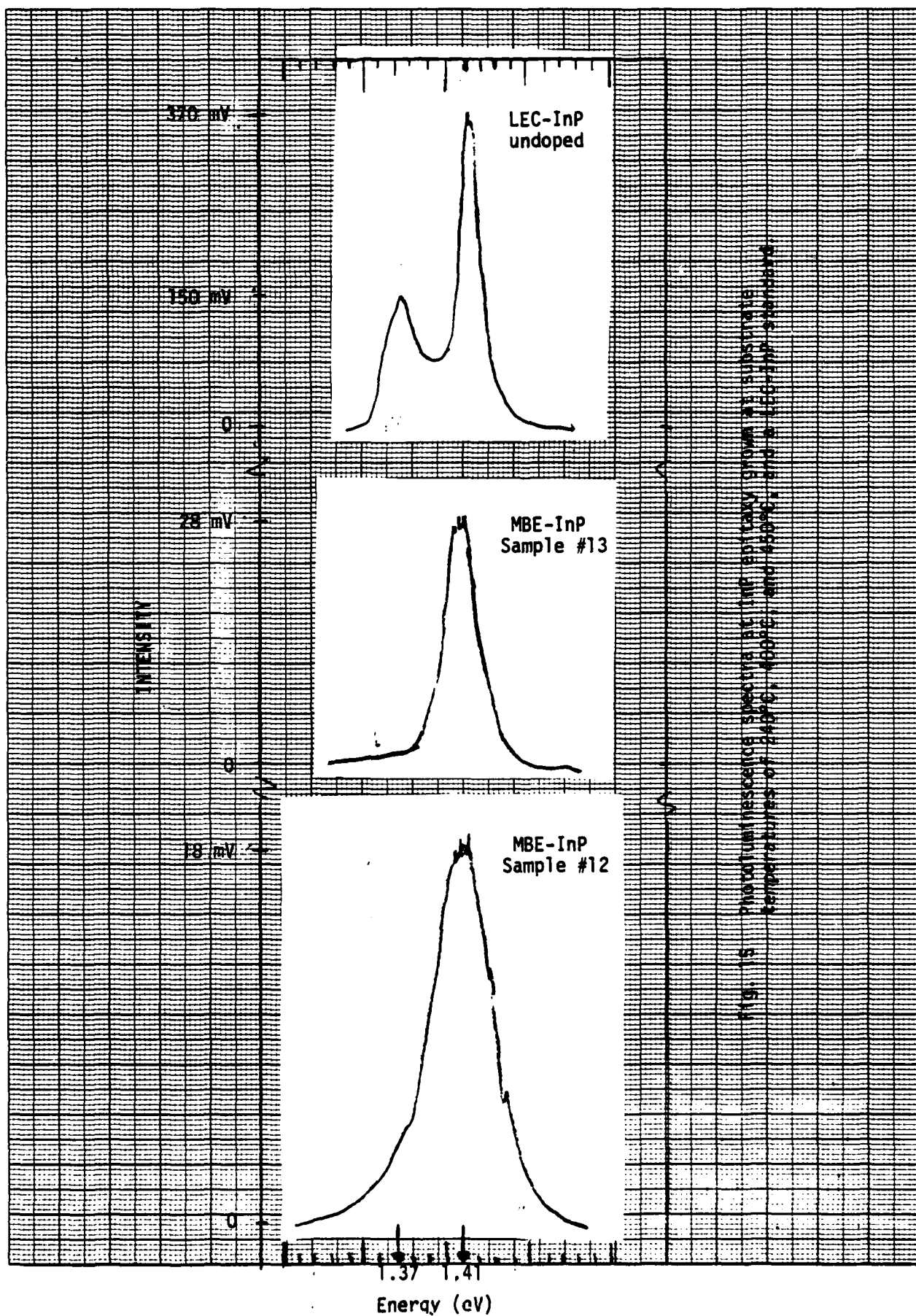


Fig. 15 Photoluminescence spectra of InP epitaxy grown on substrate temperatures of 250°C, 400°C, and 450°C.

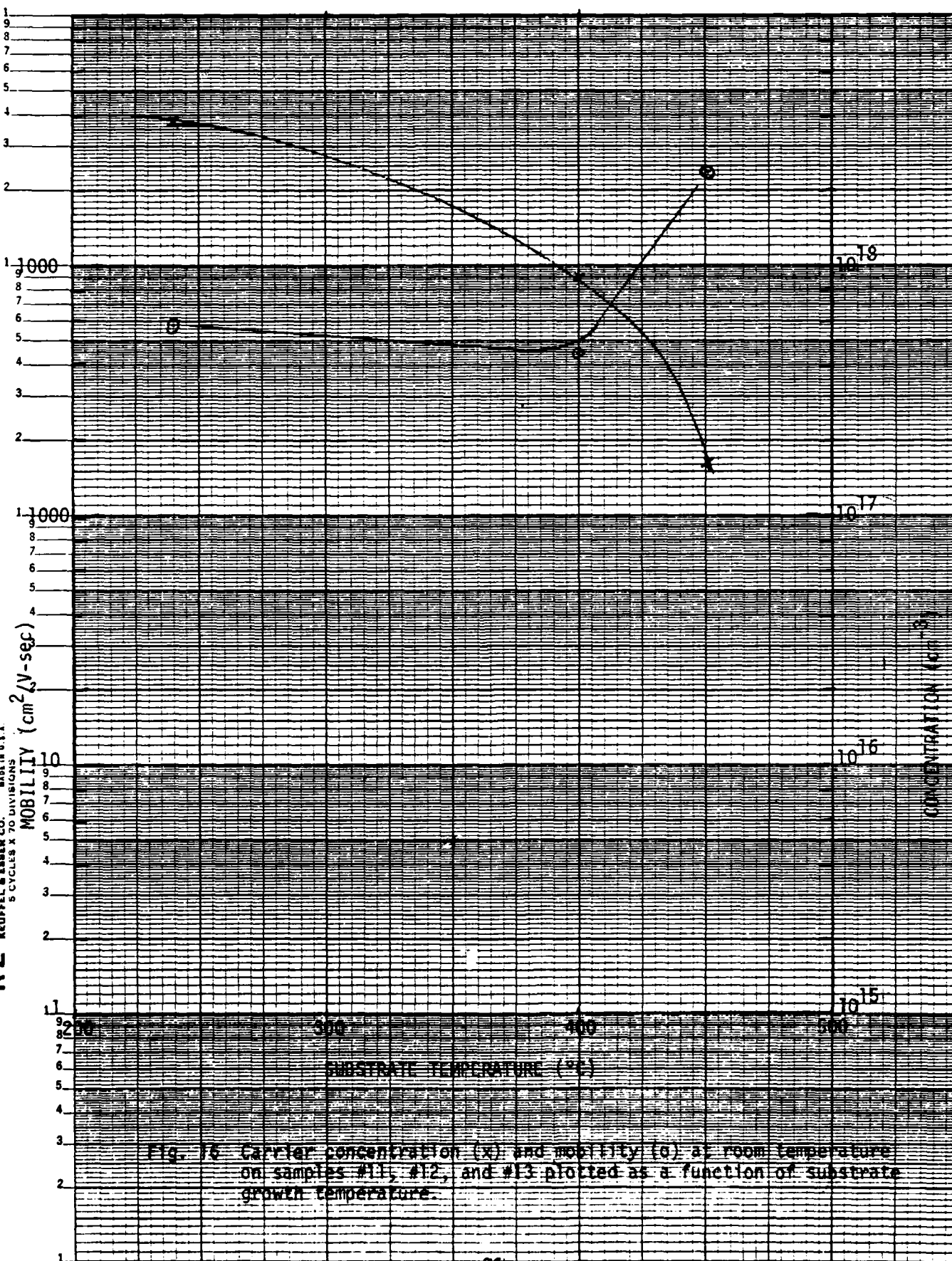
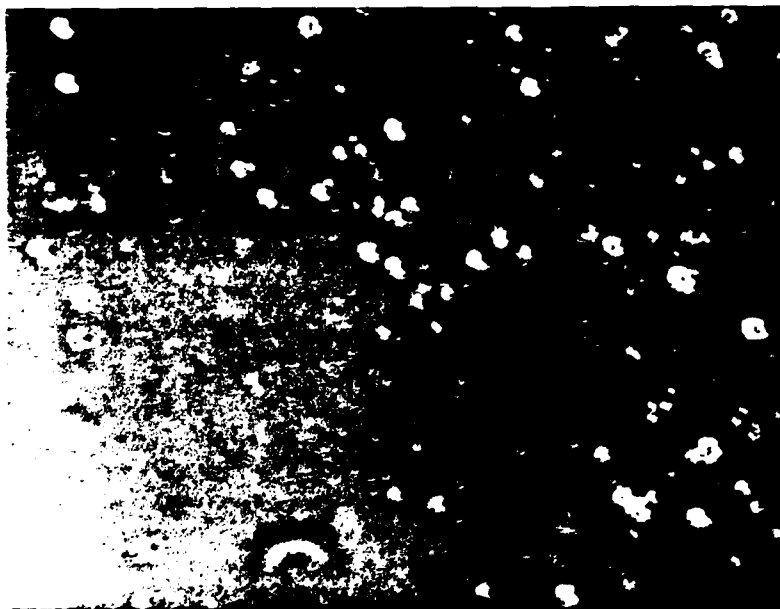


Fig. 16 Carrier concentration (x) and mobility (o) at room temperature on samples #11, #12, and #13 plotted as a function of substrate growth temperature.



Joyce et al¹⁴ reported on high-purity VPE-InP on chromium-doped InP (100) substrates (Fig. 5 of Ref. 14). Sample #13 shows a low-intensity acceptor peak at 1.37 eV, which also was reported by Kawamura et al.¹¹ Apparently for MBE-InP layers, other acceptors play a more important role in compensation.

Surface micrographs of samples #11, #12, and #13 are given in Fig. 17 and show increasing degradation with increasing substrate temperature, in spite of improved electrical and optical properties. We are probably growing in the transition to In-stabilized or in the In-stabilized surface condition, because just by raising the substrate temperature from 400°C to 450°C yields a morphology indicative of thermal etching.

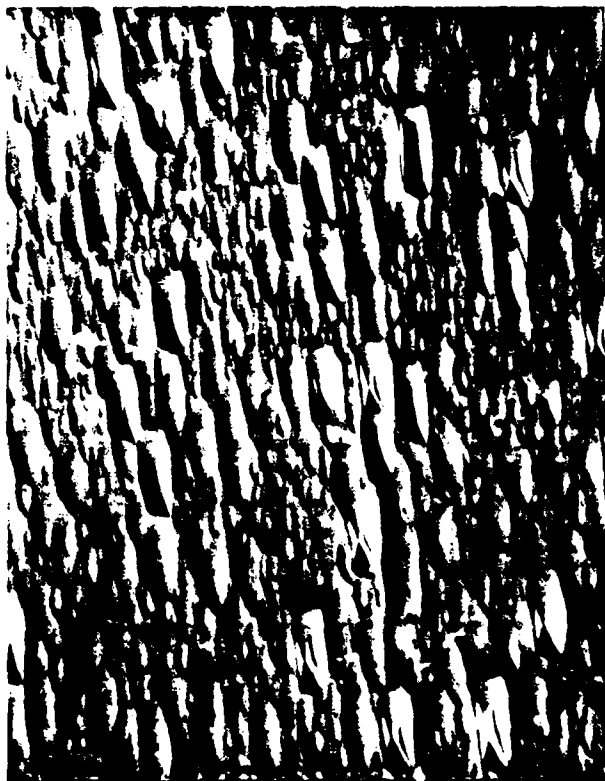


(a)
Sample #11, 900X magnification.



(b)
Sample #12, 900X magnification.

Fig. 17 Surface morphologies of InP epitaxy grown at substrate temperatures of (a) 240°C and (b) 400°C.



(c)

Sample #13, 900x magnification.

Fig. 17 Surface morphology of InP epitaxy grown at substrate temperature of 450°C.

V. SUMMARY

The following conclusions are derived from the work prescribed here:

1. When PH_3 is cracked, the phosphorus dimer is the dominant species, and very small amounts of white phosphorus are produced.
2. The nozzle furnace design has a cracking efficiency of about 37%.
3. The quartz baffle furnace design has over a 90% cracking efficiency.
4. A TaP_x compound is formed when PH_3 is passed over tantalum at temperatures $> 500^\circ\text{C}$.
5. The cracking efficiency doubles when the flow rate is increased by two orders of magnitude.
6. By increasing the substrate temperature during growth from 240°C to 450°C :
 - a. the unintentional background doping concentration decreases;
 - b. the mobility increases;
 - c. the photoluminescence peaks increase in intensity and become narrower, and
 - d. the surface morphology degrades.



VI. REFERENCES

1. R. C. H. Farrow, J. Phys. D-7, L121 (1974).
2. Y. Matsushimer, Y. Hirojuji, S. Gonda, S. Mukai and M. Kimata, Japan. J. Appl. Phys. 15, 2321 (1976).
3. J. H. McFee, B. I. Miller and K. J. Bachmann, J. Electrochem. Soc. 124, 259 (1977).
4. McBride, Heimel, Ehlers and Gorden, Thermodynamic Properties to 6000°K for 210 Substances Involving the First 18 Elements (National Aeronautics & Space Admin., Washington DC, 1963).
5. Comprehensive Inorganic Chemistry, Vol. 2, 416 (1973), contributor: A. D. F. Toy.
6. 1979 Registry of Toxic Effects of Chemical Substances, Ed. R. J. Lewis, Sr. and R. L. Tatken, NIOSH Publication No. 80-111.
7. P. E. Luscher, Solid State Technol. 20, 43 (1977).
8. R. P. Elliott, Constitution of Binary Alloys, 1st Supplement (McGraw-Hill Book Company), p. 507.
9. Mellor's Comprehensive Treatise on Inorganic and Theoretical Chemistry, Vol. VIII, Supplement III: Phosphorus (Wiley-Interscience, New York, 1971), p. 350.
10. Nils Schonberg, Acta Chemica Scandinavica, Vol 8, No. 2, 226 (1954).
11. Y. Kawamura, M. Ikeda, H. Asahi, H. Okamoto, Appl. Phys. Lett. 35(7), 481 (1 Oct 1979).
12. J. S. Roberts, P. Dawson, G. B. Scott, Appl. Phys. Lett. 38(11), 905 (1 June 1981).
13. D. L. Rode, Phys. Rev. B, Vol. 3, No. 10, 3287 (1971).
14. B. D. Joyce and E. W. Williams, Proc. 3rd International Symp. on GaAs and Related Compounds, Institute of Physics, 57 (1970).



APPENDIX A: HANDLING OF COMPRESSED PH_3 GAS CYLINDERS

i. Handling of Cylinders

- A. Use only in well ventilated areas, preferably under a hood with forced ventilation.
- B. Keep valve protection cap on until cylinder is secure and ready for use.
- C. Transport cylinders with a suitable hand truck.

ii. Storage of Cylinder

- A. Store cylinder in a cool ($<52^\circ\text{C}$) dry, well-ventilated area of noncombustible construction.
- B. Store cylinders in upright position.
- C. Isolate cylinder from highly oxidizing materials (halogens and oxygen).

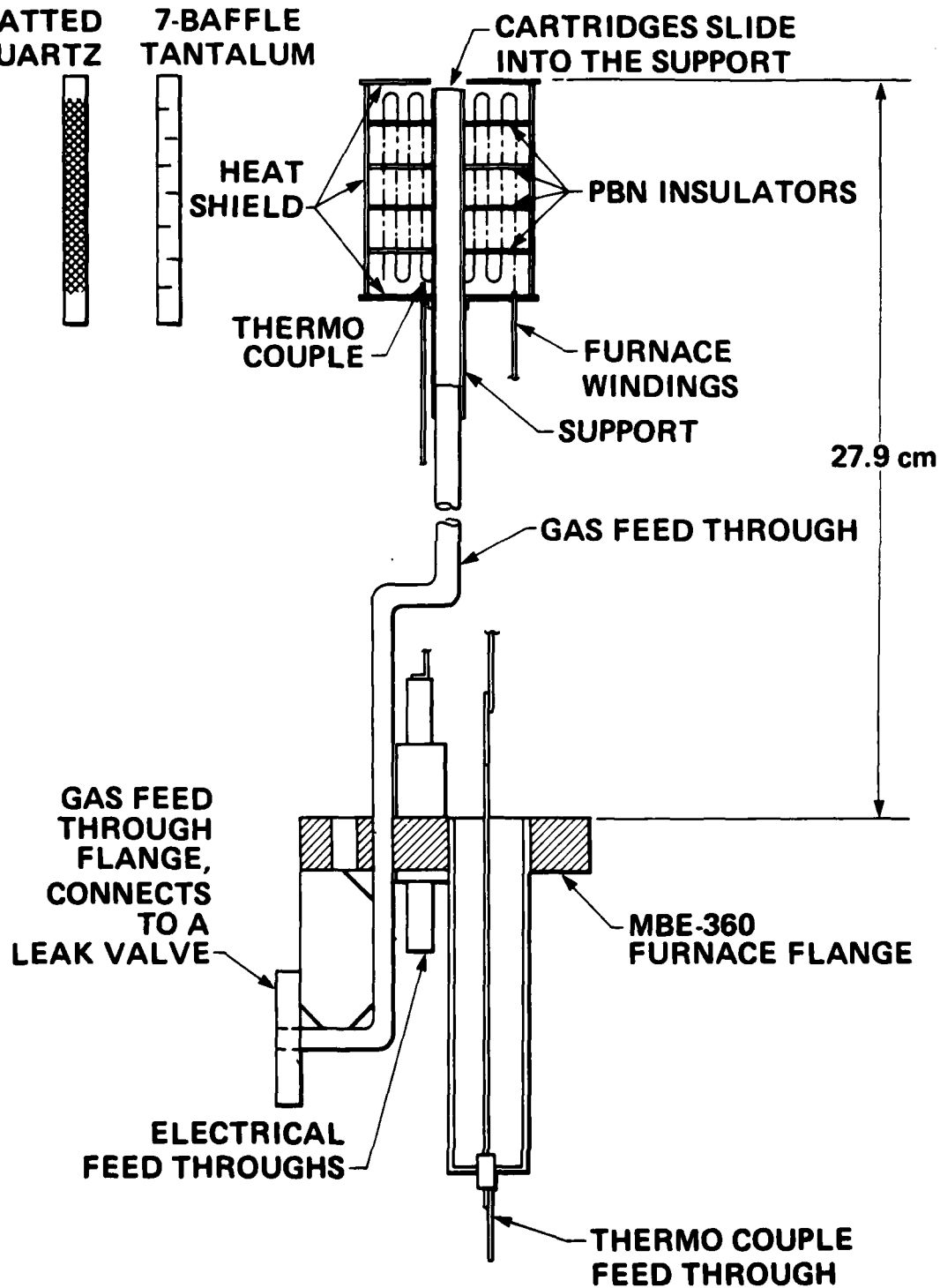
iii. Normal Usage

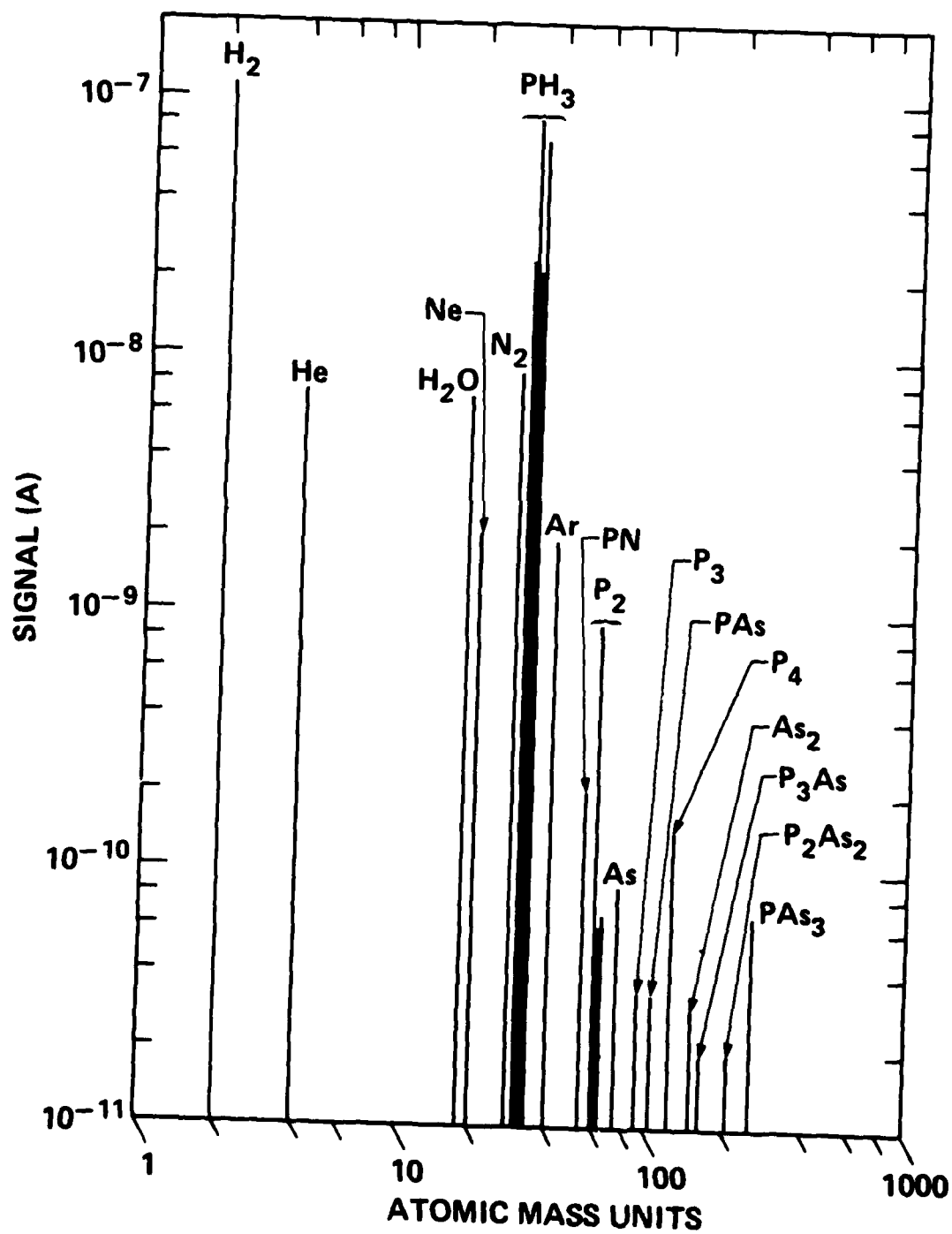
- A. Leak check vacuum station with He regularly.
- B. Work with another person who is familiar with the apparatus.
- C. Wear lab coats.
- D. Wash hands and face after touching the cylinder.

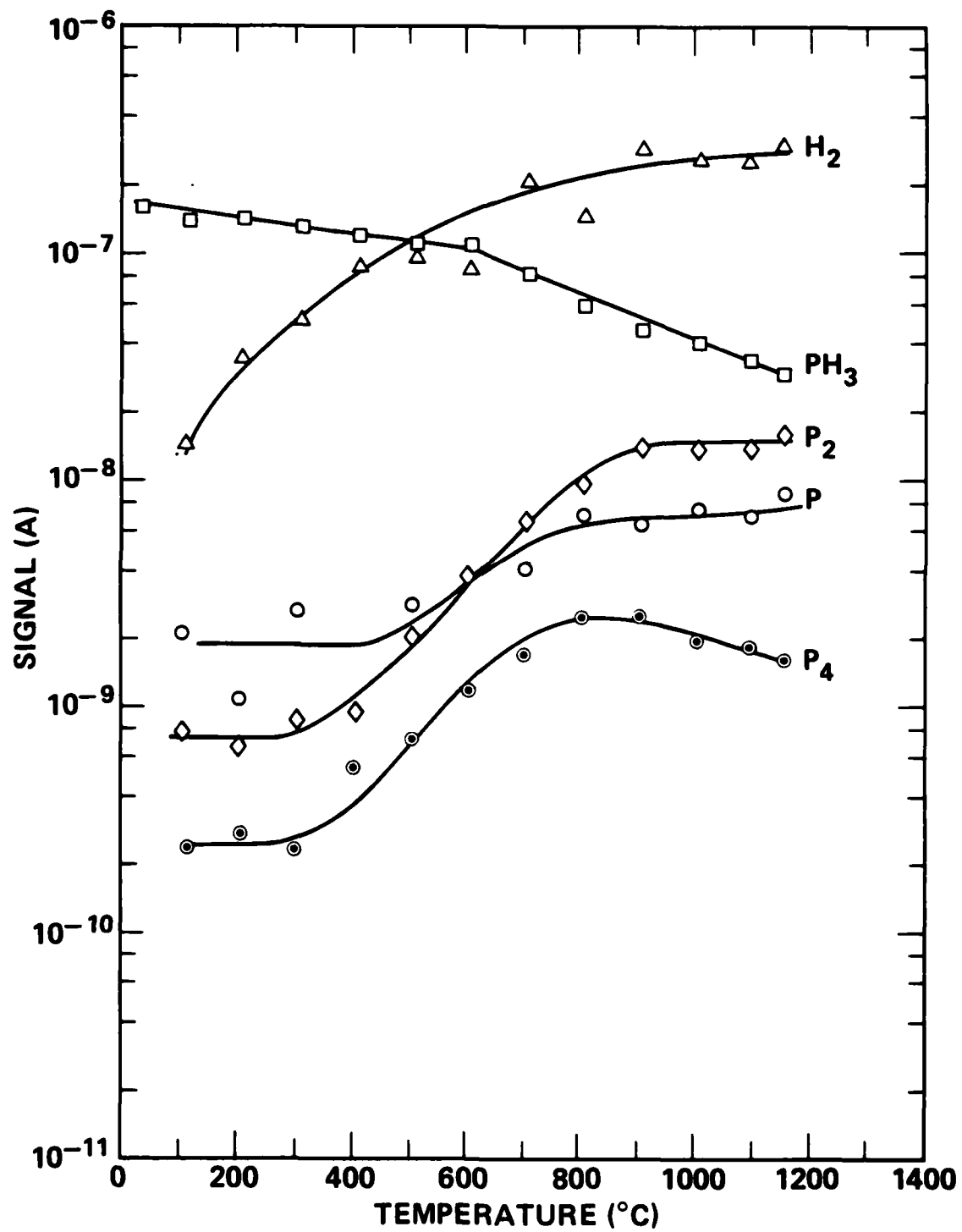
iv. Emergency Release

- A. Clear immediate vicinity.
- B. Close lab doors.
- C. Trigger the building alarm system.
- D. If leak (fire) is small (inside hood), test with gas detector.
 - 1. Wear self-contained respirator.
 - 2. Test with gas detector and re-enter lab.
 - 3. Close the necessary valves.
 - 4. Leave area.

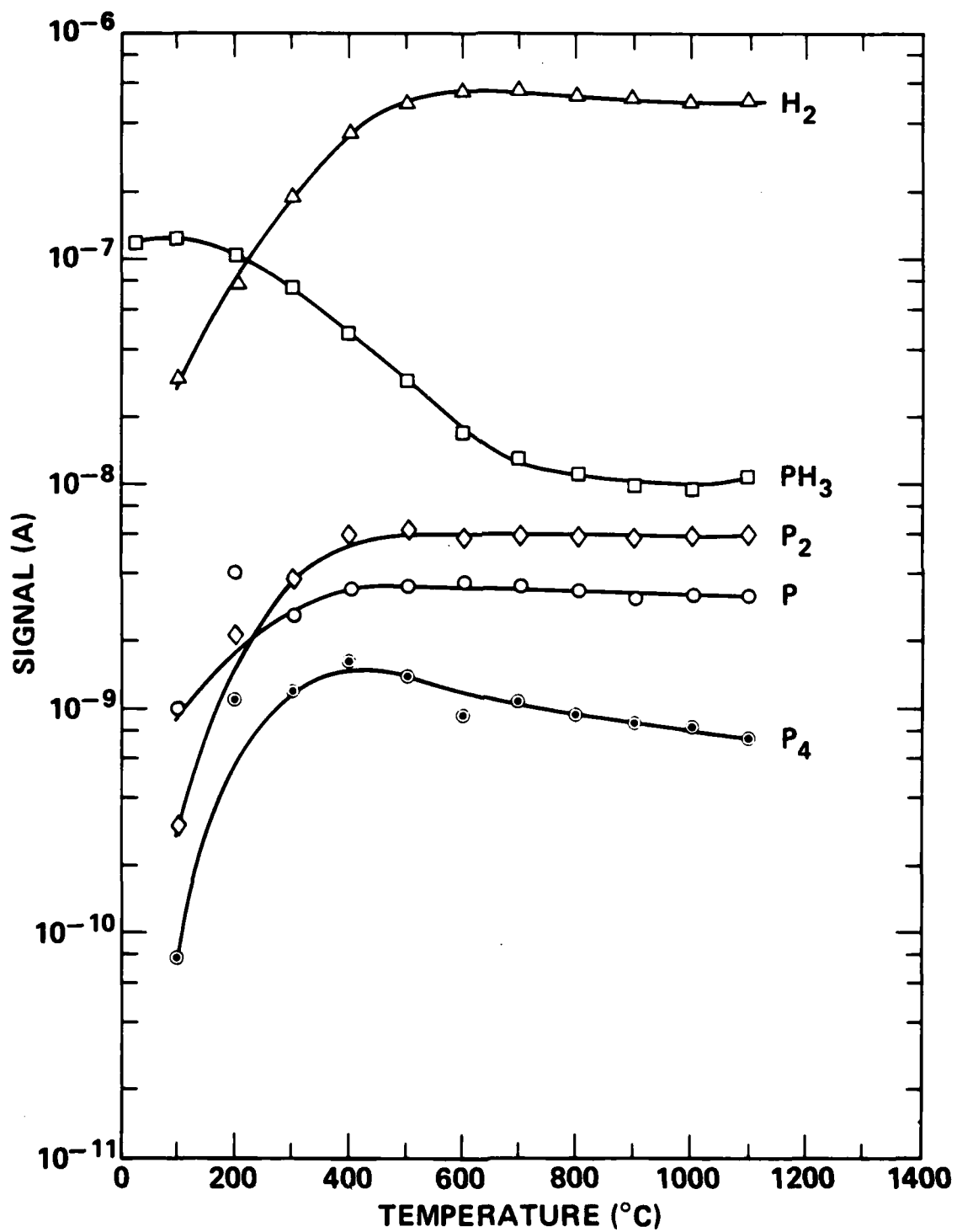
CARTRIDGES:
MATTED **7-BAFFLE**
QUARTZ **TANTALUM**



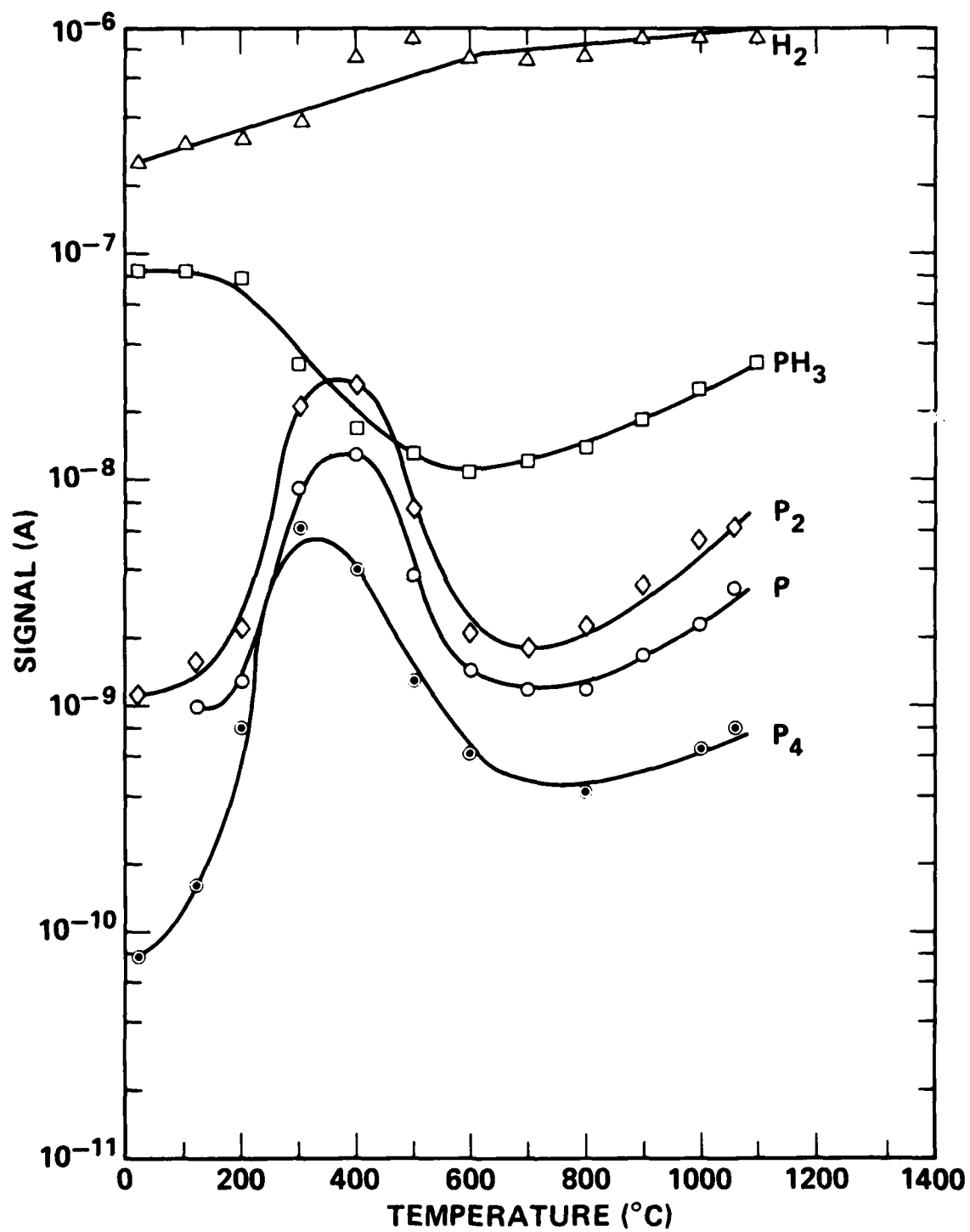




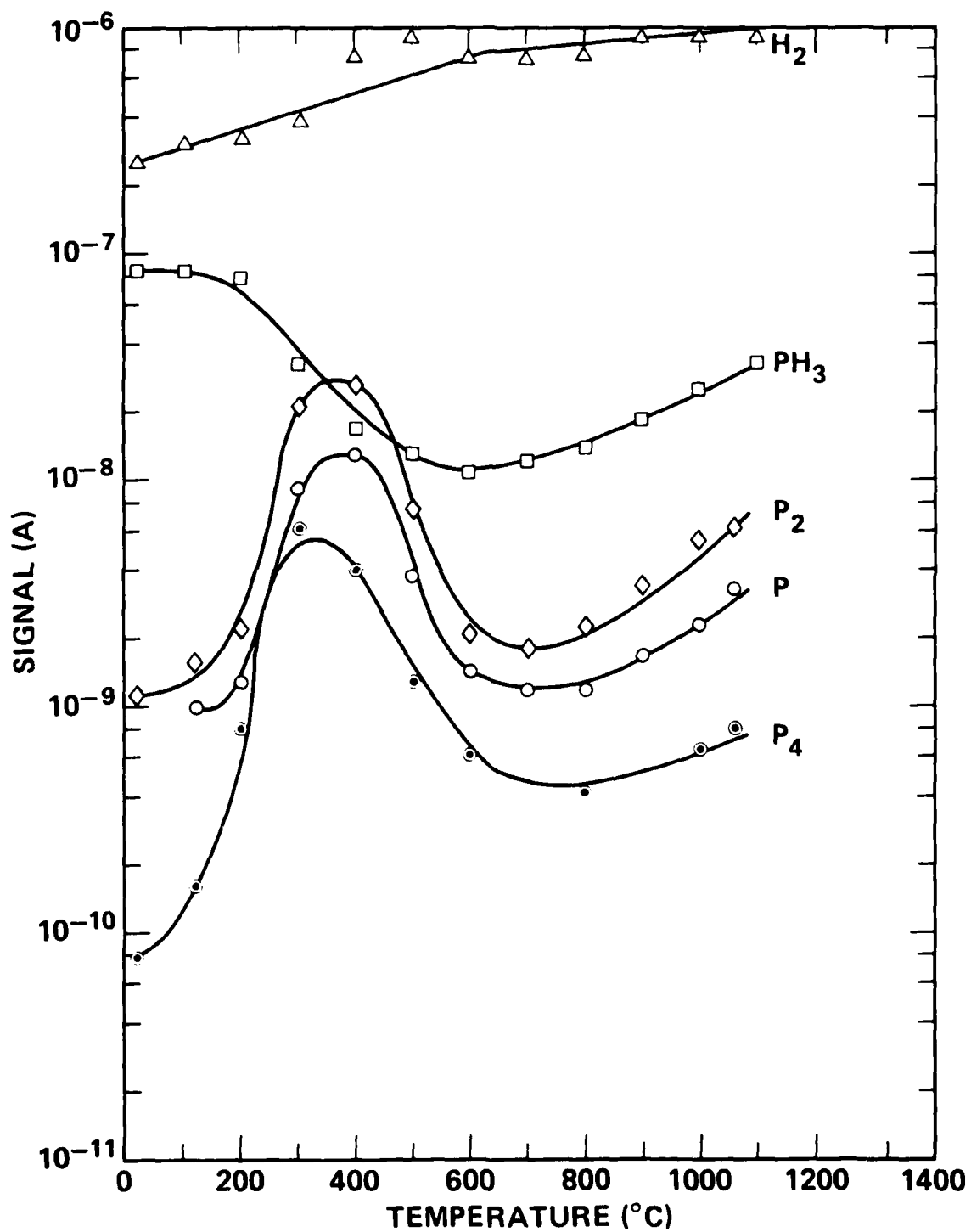
ZERO-BAFFLE QUARTZ CARTRIDGE



**MATTED QUARTZ-FILLED QUARTZ
CARTRIDGE**



7-BAFFLE TANTALUM CARTRIDGE



7-BAFFLE TANTALUM CARTRIDGE

ATE
LMED
-83